


## Stability and Asymmetry of Tide-Influenced River Bifurcations

A. P. Iwantoro<sup>1</sup> , M. van der Vegt<sup>1</sup> , and M. G. Kleinhans<sup>1</sup> 

<sup>1</sup>Department of Physical Geography, Faculty of Geosciences, Utrecht University, Utrecht, The Netherlands

### Key Points:

- Tides affect the range of parameters for which symmetric bifurcations can persist
- Stable symmetric bifurcations are more likely for intermediate tidal influence than for small or large tidal influence
- Tide-influenced bifurcations are less asymmetric compared to their river-dominated counterparts

### Correspondence to:

A. P. Iwantoro,  
a.p.iwantoro@uu.nl

### Citation:

Iwantoro, A. P., van der Vegt, M., & Kleinhans, M. G. (2022). Stability and asymmetry of tide-influenced river bifurcations. *Journal of Geophysical Research: Earth Surface*, 127, e2021JF006282. <https://doi.org/10.1029/2021JF006282>

Received 31 MAY 2021

Accepted 28 MAY 2022

### Author Contributions:

**Conceptualization:** A. P. Iwantoro, M. van der Vegt, M. G. Kleinhans  
**Data curation:** A. P. Iwantoro  
**Formal analysis:** A. P. Iwantoro, M. van der Vegt  
**Funding acquisition:** A. P. Iwantoro  
**Investigation:** A. P. Iwantoro  
**Methodology:** A. P. Iwantoro, M. van der Vegt, M. G. Kleinhans  
**Project Administration:** M. van der Vegt, M. G. Kleinhans  
**Resources:** M. G. Kleinhans  
**Software:** A. P. Iwantoro  
**Supervision:** M. van der Vegt, M. G. Kleinhans  
**Validation:** A. P. Iwantoro  
**Visualization:** A. P. Iwantoro  
**Writing – original draft:** A. P. Iwantoro  
**Writing – review & editing:** M. van der Vegt, M. G. Kleinhans

© 2022. The Authors.

This is an open access article under the terms of the [Creative Commons Attribution License](https://creativecommons.org/licenses/by/4.0/), which permits use, distribution and reproduction in any medium, provided the original work is properly cited.

**Abstract** Bifurcations are important geomorphological features in tide-influenced deltas. At bifurcations, river flow and tides distribute sediment over the channel network and determine the morphodynamic evolution of the entire delta. Using a one-dimensional numerical model, we study the effects of tides on the morphological evolution of bifurcations from river-dominated to tide-dominated systems. In accordance with previous studies, bifurcations with small tidal influence, in which the flood flow hardly drives morphological change, have a larger range of Shields stress and width-to-depth ratio conditions for which symmetric bifurcations are stable to depth perturbations, compared to their river-dominated counterparts. We extended the existing studies to tide-dominated conditions. When bifurcations become increasingly tide-dominated, the range of conditions under which balance discharge partition (symmetric morphology) can exist, shrinks. Under these conditions, the bed can also change during the flood phase and growth of the bed asymmetry is larger than the decay during ebb. However, the bed asymmetry in equilibrium becomes less pronounced with increasing tidal dominance. We conclude that tides reduce the tendency of closure and abandonment of one of the downstream channels compared to river-dominated bifurcations, either by inhibiting the instability or by reducing asymmetry.

**Plain Language Summary** River deltas often have multiple river branches through which water and sand flow. These branches are connected at bifurcations, where one upstream channel splits in two downstream channels. In rivers, bifurcations often tend to evolve asymmetrically such that one of the branches silts up while the other enlarges. This asymmetry often leads to abandonment of one of the branches. However, deltas where tidal currents are important rarely show a channel abandonment, for which reasons are not yet fully understood. Here we present a numerical model with which we investigated bifurcation stability, ranging from river-dominated to tide-dominated. The main finding is that even though a strong tidal influence in the delta increases the possible conditions for bifurcations to be asymmetric, this asymmetry is much less pronounced than in river-dominated deltas. Results presented in this work help to explain the existence of multiple active river branches in tide-influenced deltas.

## 1. Introduction

Bifurcations are common features in fluvial systems, where a larger upstream channel splits into two smaller downstream channels and can be found in steep slope rivers as well as in lowland rivers and deltas. In the fluvial-dominated channel networks, river flow divides at bifurcations and determines the sediment distribution as well as the morphodynamics of the downstream channels. In these systems, one of the downstream channels of a bifurcation is often abandoned, resulting in one dominant downstream channel that conveys the river discharge (Bolla Pittaluga, Coco, et al., 2015; Kleinhans et al., 2008). In the tide-influenced systems, tides cause a change in flow magnitude during ebb and even change the system into a confluence during flood if tides are large enough, suggesting that bifurcations in these systems may develop differently. Hoitink et al. (2017) suggested that such channel abandonment rarely occurs in tide-influenced systems, keeping both downstream channels open to convey the water. In this paper we investigate the effect of tides on the stability and asymmetry of bifurcations as found in tide-influenced river deltas.

Morphodynamics of river-dominated bifurcations have been thoroughly studied for a range of settings in river systems, from low sediment mobility in gravel bed rivers (Bertoldi & Tubino, 2007; Bolla Pittaluga, Coco, et al., 2015; Bolla Pittaluga et al., 2003) to high sediment mobility rivers (Bolla Pittaluga, Coco, et al., 2015; Edmonds & Slingerland, 2008; Slingerland & Smith, 1998). It was found that symmetric bifurcations are unstable in high and low sediment mobility (Shields stress), resulting in asymmetric bifurcations and abandonment of

one of the downstream channels. Only a limited mid-range of sediment mobility conditions exists that results in stable symmetric bifurcations. The stability of symmetric bifurcations also depends on width-to-depth ratio of the upstream channel. Bifurcations with larger width-to-depth ratio have a more limited range of sediment mobility for which stable symmetric bifurcations can exist (Bolla Pittaluga, Coco, et al., 2015; Redolfi et al., 2016, 2019). Some studies have addressed effects of different geomorphological features in river systems. Meandering of the upstream channel enhances the asymmetry between downstream channels (Kleinhans et al., 2008; Slingerland & Smith, 1998), migrating bars increases the dynamics of bed level of bifurcations (Bertoldi et al., 2009), and evolving river banks increase the conditions for asymmetric downstream channels (Kleinhans et al., 2011; Miori et al., 2006). Furthermore, Salter et al. (2017) showed that the asymmetric morphological development of bifurcations in river dominated deltas can be controlled by the presence of downstream sediment sinks. Sediment deposition at a shallow estuary-shelf boundary will result in channel lengthening. This will shift the asymmetry evolution of the bifurcation, where the lengthened channel will silt up and the shallow channel will deepen, whereupon this channel will lengthen. This shifting asymmetry evolution will continue until the estuary-shelf transition is in very deep water.

The stability and morphodynamics of tide-influenced bifurcations are much less clear. Though observations demonstrate the existence of seemingly stable, nearly symmetric bifurcations in tide-influenced deltas such as in Mahakam Delta (Sassi et al., 2013) and Berau River Delta (Buschman et al., 2013), some observations also found highly asymmetric bifurcations (e.g., Chen et al., 1982; Kästner & Hoitink, 2019). Based on a two-dimensional (2DH) modeling study, Iwantoro et al. (2020) found that bifurcations are less asymmetric for tide-dominated rivers because tide-induced flows tend to partition less asymmetrically than river-induced flow velocities. However, they only simulated a small range of sediment mobility, tidal influence and width-to-depth ratio conditions applied in 13 simulations and in many cases the asymmetry was externally forced by differences in either channel length or tidal forcing. They were also not able to find stable symmetric bifurcations. Simulating a full deltaic channel network by using a 2DH numerical model, Rossi et al. (2016) found that delta systems with stronger tidal influence have a more stable morphology resulting in a less frequent avulsion. Using physical laboratory experiments, Lentsch et al. (2018) confirmed the finding of Rossi et al. (2016) and suggested that the same results will occur under sea level rise conditions. However, they only simulated a limited range of tidal amplitudes and sediment sizes, and did not systematically vary the sediment mobility and width-to-depth ratio that were shown to be important parameters for the morphodynamics of bifurcations in river dominated systems (e.g., Bolla Pittaluga, Coco, et al., 2015; Redolfi et al., 2019). In a recent study, Ragno et al. (2020) showed that symmetric bifurcations are stable to bed perturbations for a wider range of Shields stress and width-to-depth ratio values when tides are added to a river system. This is caused by the increased flow velocity in a tidal cycle, which deepens both downstream channels, reduces the width-to-depth ratio, and reduces the asymmetry between them. However, Ragno et al. (2020) studied small tide conditions in which tides only cause a fluctuation in river flow magnitude but no flow reversal during a tidal cycle. Besides, they also applied a straight channel while in tidal systems a converging channel width is more common (e.g., Davies & Woodroffe, 2010; Fagherazzi & Furbish, 2001; Langbein, 1963; Lanzoni & Seminara, 1998; Savenije, 2015). As a result, it is still unclear how tides affect the asymmetry of tide-dominated bifurcations for a wide range of Shields stress conditions and width-to-depth ratios.

To extend our knowledge about the morphodynamics of tide-influenced bifurcations, in this study we aim to determine the effects of tides on (a) the stability and (b) the asymmetry in morphodynamic equilibrium of tide-influenced bifurcations, from small tidal influence that results in a changing flow magnitude, to tide-dominated conditions at which the flow is bi-directional. To achieve this objective, the one-dimensional (1D) morphodynamic numerical model of Iwantoro et al. (2021) was applied to tidal systems. The model was adapted such that flow and sediment transport at the bifurcation can change in magnitude and direction. Though a 1D model is not as capable to simulate the detailed flow conditions and morphology as 2D or 3D models (e.g., Edmonds & Slingerland, 2007, 2008; Kleinhans et al., 2008; Rossi et al., 2016) or physical models (e.g., Bertoldi et al., 2009; Bertoldi & Tubino, 2007; Lentsch et al., 2018), 1D models have been widely applied to study long-term morphodynamic evolution of rivers, estuaries and deltas (e.g., Bolla Pittaluga, Tambroni et al., 2015; Salter et al., 2017, 2020). The advantage of the 1D approach is that it is computationally less expensive than 2D and 3D approaches, but still capable to explain the important processes that drive the morphodynamic evolution of bifurcations (e.g., Bolla Pittaluga, Coco, et al., 2015; Iwantoro et al., 2021; Ragno et al., 2020; Redolfi et al., 2019). As a result, a broader range of conditions that exists in nature could be studied in a much shorter

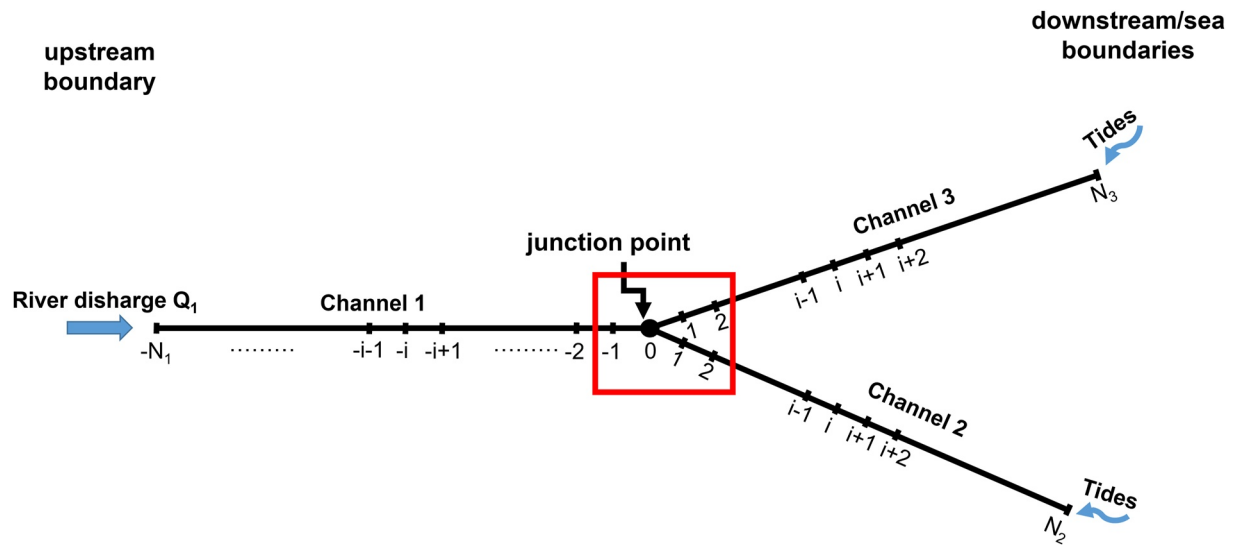


**Figure 1.** Illustration of bifurcation model domain and boundary conditions. Channel 1 is the upstream channel and is forced by river discharge from upstream boundary, while Channel 2 and Channel 3 are the downstream channels that are forced by time-varying water levels at the downstream boundary. The three channels are connected at the junction point/boundary.

computational time than with the other approaches. We limit our study to deltas that have a sandy bed, thereby ruling out muddy systems, which need a different approach to model sediment transport.

A single bifurcation was studied at which three channels connect (Figure 1). The two downstream channels were forced by tides from the downstream boundary, while at the upstream channel a steady river discharge was prescribed. Sets of simulations were prepared to simulate the morphodynamics of bifurcations with different tidal influence. This was achieved by changing discharge, tidal range and the geometry of the system (width profile). The detailed approach is described in Section 2. Then the results and the explanation of the basic mechanisms that drive the morphodynamical evolution tide-influenced bifurcation are provided in Section 3. The results, limitations and future studies are discussed in Section 4, and finally the conclusions of this study are presented in Section 5.

## 2. Methodology

### 2.1. Model Description

#### 2.1.1. Hydrodynamics

The Saint Venant equations were solved to compute the hydrodynamics (Cunge et al., 1980). This approach is more suitable for this study than other approaches, such as locally uniform flow (Salter et al., 2017) or the back-water equations (Kleinhans et al., 2008) because tides cause unsteady flow. The following equations were solved:

$$w \frac{\partial z}{\partial t} + \frac{\partial Q}{\partial x} = 0 \quad (1)$$

$$\frac{\partial Q}{\partial t} + \frac{\partial}{\partial x} \left( \frac{Q^2}{A} \right) + gA \frac{\partial z}{\partial x} + \frac{|Q|QP}{C^2 A^2} = 0, \quad (2)$$

in which  $x$  and  $t$  are the spatial and temporal axes and  $Q$  is the discharge caused by river flow and tides. Furthermore,  $w$  is the channel width and  $A$  and  $P$  in Equation 2 are the cross-sectional area and wetted perimeter of the channel, respectively. The model assumes that the presence of tidal flats is negligible. Therefore,  $w$  is constant in the entire tidal cycle. This assumption is considered plausible because many tidal systems has limited tidal flat that are insignificant to the flow dynamics in the channel such as in Mahakam Delta, Berau River Delta and Mekong River Delta. By assuming that the channels have a rectangular cross section,  $A$  is calculated by  $A = w(z - \eta) = wh$ , where  $\eta$  is the bed level,  $z$  is water level and  $h$  is water depth. Meanwhile, we approximate here that

$P = w$ , therefore  $P/A$  in the friction term in Equation 2 equals  $1/h$ , and the friction term does not depend on the width-to-depth ratio. By doing this the hydrodynamics and morphodynamics of the system are independent of the width as long as the prescribed specific discharge upstream is not changed between simulations. This allows for studying the sensitivity of the results to the width-to-depth ratio without changing the equilibrium bathymetry. Finally,  $g$  is the gravitational acceleration and  $C$  is Chézy coefficient, related to roughness by

$$C = 18 \log_{10}(12h/\xi) \quad (3)$$

where  $\xi$  is the Nikuradse roughness length related to the presence bedforms (van Rijn, 1984a).

Two kinds of boundary nodes are present, namely open boundaries and junction boundaries. Open boundaries are located at the upstream node of the upstream channel (upstream boundary in Figure 1) and at the downstream node of the downstream channels (downstream boundary in Figure 1). The junction boundary is a node shared by three connected channels at the bifurcation, known as nodal point. At the upstream boundary, equilibrium river discharge was prescribed as follows

$$Q_{1;ub} = w_{1;ub} C h_1 \sqrt{g h_1 S_1} \quad (4)$$

where the subscripted number defines the channel identity as in Figure 1,  $w_{1;ub}$  is the channel width at upstream boundary and  $S$  is channel slope ( $\text{m m}^{-1}$ ).

At the downstream boundaries, water level is prescribed as

$$z = z_0 + \sum_{k=1}^N a_k \cos(\omega_k t + \varphi_k) \quad (5)$$

where  $z_0$  is the mean mean water level ( $z_0 = 0$  here),  $a_k$  and  $\varphi_k$  are amplitude and phase of the tidal constituent  $k$ , and  $\omega_k = 2\pi/T_k$ , in which  $T_k$  is tidal period of constituent  $k$ . Here, we only prescribed one tidal constituent at the seaward boundary, but in principle multiple constituents can be prescribed.

Defining the junction boundary to be located at  $x = 0$ , and positive  $x$  in downstream direction, the discharge at the junction satisfies the conservation of mass as follows

$$Q_1(0, t) = Q_2(0, t) + Q_3(0, t) \quad (6)$$

while the water level was assumed to be equal, neglecting the effect of dynamic pressure:

$$z_1(0, t) = z_2(0, t) = z_3(0, t) \quad (7)$$

Because the dynamic pressure was neglected, the water level difference between the channels at the junction due to energy dissipation by turbulence as used, for example, in Edmonds and Slingerland (2008), Gurram et al. (1997), Ragno et al. (2021), is neglected. The hydrodynamic calculations were solved using an implicit Preissmann scheme (see Cunge et al., 1980 for details). The scheme is unconditionally stable. Therefore, the time steps can be independently defined to optimize the spatial accuracy and computational capacity.

### 2.1.2. Sediment Transport and Morphodynamics

The sediment transport is based on van Rijn (1984a, 1984b) and is applicable in the range of sand and gravel. It computes the bedload and suspended load separately. The details of the sediment transport equations applied in the 1D model can be found in Iwamoto et al. (2021). The applied sediment transport model assumes local flow and transport are in equilibrium and neglects time lags that may occur between peak flow and sediment transport (Groen, 1967) as well as a spatial settling lag (Postma, 1961) that typically occurs in tide-influenced systems. We applied this simplification because of two reasons. First, we would like to keep the computation in the model as simple as possible and focus on how tides can affect the morphological evolution of bifurcations. Second, the time and spatial settling lag are mainly important for fine-grained sediment like mud (e.g., Pritchard & Hogg, 2003; van Straaten & Kuenen, 1958), while in this study we use sand. For very fine sand of 70 microns (smallest value used in this study) the settling velocity ( $w_s$ ) is around 0.4 cm/s and for the water depth of 5 m the settling time scale ( $h/w_s$ ) is around 20 min, which, although not very small, is considerably less than the semidiurnal time scale. Therefore, the assumption to neglect these lag effects are plausible for sandy systems as studied here.

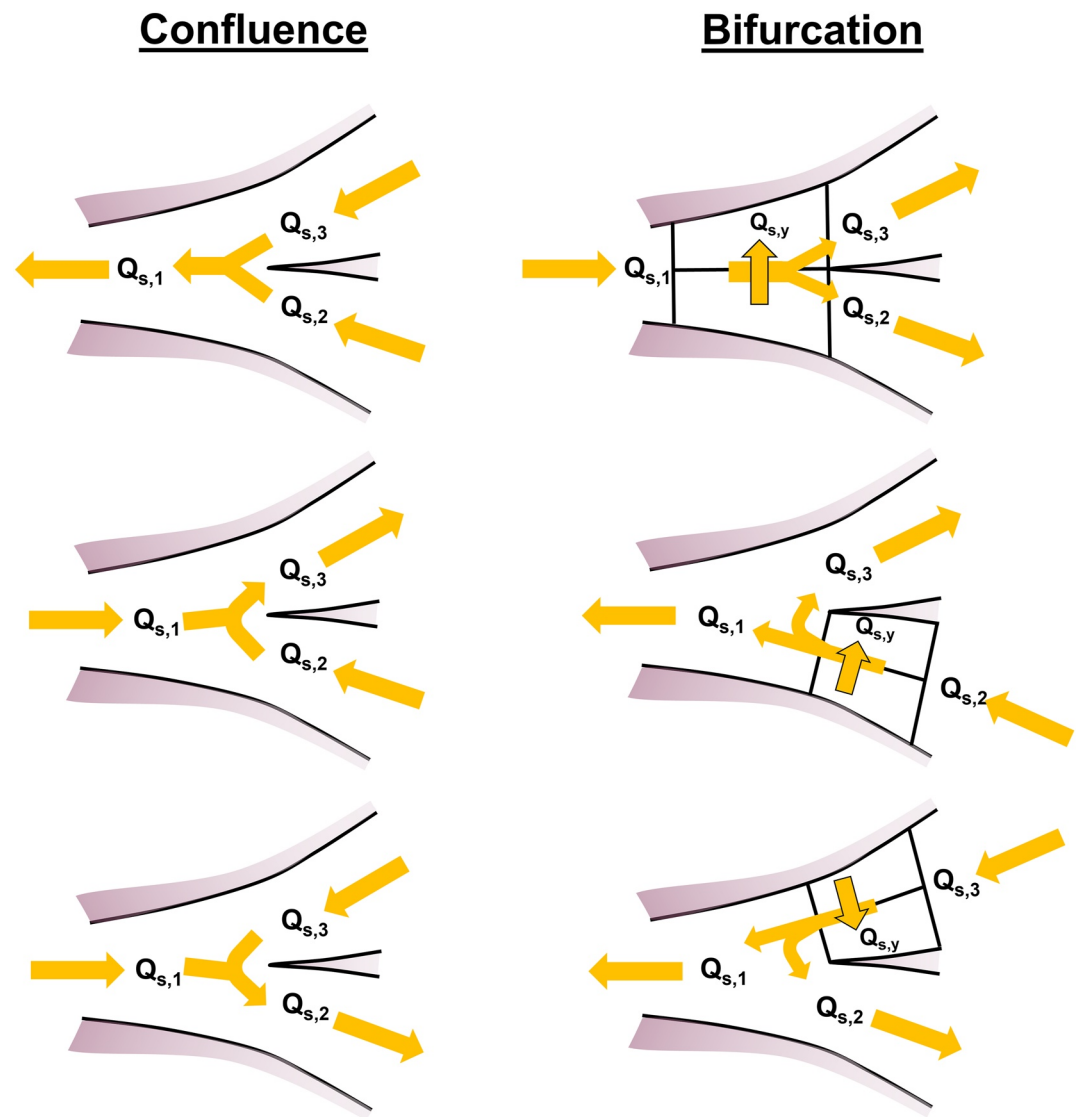


**Figure 2.** All six possible flow-induced sediment transport conditions for a tide-influence bifurcating channel. The arrow indicates the sediment transport direction for each condition. The left conditions are for the confluence conditions and the right conditions are for the bifurcation conditions.

Compared to Iwantoro et al. (2021) the main difference is the calculation of sediment transport at the junction. For tide-influenced conditions, the sediment transport direction depends on the phase of tidal currents in the branches (it can be ebb or flood flow in each channel and timing of ebb and flood is not necessarily the same in each channel) and the junction can behave as a bifurcation or as a confluence. There are three possible conditions under which the junction behaves as a bifurcation and three for which the junction is a confluence, as illustrated in Figure 2. The conditions depicted in the lower two rows of Figure 2 can occur because of different phase of the flow at the junction, causing a timing difference in ebb and flood at the junction. This can itself have many reasons, like a difference in bed level between the downstream channels, different channel lengths, difference in amplitude or phase at the seaward boundaries (Iwantoro et al., 2020) and these time differences have been observed in deltas, such as in Berau River Delta (Buschman et al., 2013) and Wax Lake Delta (Wagner & Mohrig, 2019). When the flow merges the system is a confluence and the sediment transport to the channel that receives the sediment (sink channel) is calculated by adding the sediment transport from the other two channels:

$$Q_{s,out} = Q_{s,inp1} + Q_{s,inp2} \quad (8)$$

$Q_{s,out}$  is sediment transport in sink channel while  $Q_{s,inp1}$  and  $Q_{s,inp2}$  is sediment transport from the channels that distribute the sediment transport (source channels). Meanwhile, when the flow bifurcates, the sediment transport from one source channel distributes to two sink channels:

$$Q_{s,inp} = Q_{s,out1} + Q_{s,out2} \quad (9)$$

Hence, during bifurcation conditions an expression is needed that describes how the sediment of the source channel is distributed over the two sink channels. This is the so-called nodal point relationship and previous studies have shown that results critically depend on it (Wang et al., 1995).

Here, we applied the same nodal point relationship as used in Iwantoro et al. (2021), which was based on the nodal point relationship of Bolla Pittaluga et al. (2003). The main difference here is that, depending on the flow condition, the input channel is different. This is also depicted in Figure 2 by the splitting of the last cells in the source channel. In this area a transverse sediment transport is calculated. Basically, the along channel sediment transport divides according to the width of each sink channel, plus a correction term  $Q_{s,y}$  caused by transverse suspended load transport ( $Q_{susp,y}$ ) and transverse bedslope driven bedload transport ( $Q_{bedl,y}$ ):

$$Q_{s,y} = Q_{bedl,y} + Q_{susp,y} \quad (10)$$

where

$$Q_{bedl,y} = Q_{bedl,x} \left( \frac{Q_y h_{inp}}{Q_{inp} \alpha h_{123}} - \frac{r}{\sqrt{g'_{inp}}} \frac{\partial \eta}{\partial y} \right) \quad (11)$$

while  $Q_{susp,y}$  is expressed by

$$Q_{susp,y} = Q_{susp,x} \left( \frac{Q_y h_{inp}}{Q_{inp} \alpha h_{123}} \right) \quad (12)$$

Here,  $Q_{bedl,x}$  and  $Q_{susp,x}$  are along-channel bedload and suspended load transport from the source channel at the junction, respectively. The transverse bedload transport is affected by both transverse flow (first term on the righthand side), which occurs because one of the two sink channels receives relatively more water than the other, and by transverse bedslope effect (second term on the righthand side). The transverse suspended load transport is only affected by the transverse flow. In Equations 11 and 12,  $Q_{inp}$  is discharge in the source channel and  $Q_y$  is transverse discharge computed by

$$Q_y = \frac{1}{2} \left( Q_{out1} - Q_{out2} - Q_{inp} \frac{W_{out1} - W_{out2}}{W_{out1} + W_{out2}} \right) \quad (13)$$

where  $Q_{out1}$  and  $Q_{out2}$  are the water discharge in the two sink channels. Note that when the discharge divides at the bifurcation proportional to the respective widths of the sink channels,  $Q_y = 0$ . In Equations 11 and 12,  $\alpha$  is the dimensionless length (scaled by channel width of the input channel) of the region of influence of the bifurcation and determines over which distance from the junction the transverse transport in the source channel occurs. Bolla Pittaluga et al. (2003) suggested that  $\alpha$  is between 2 and 3. From physical experiments, Bertoldi and Tubino (2007) suggested that  $\alpha$  has an optimum value of 6. However, Redolfi et al. (2019) found that the value of  $\alpha$  depends on the Shields stress and friction coefficient. We used  $\alpha = 3$ . Moreover, the constant  $r$  in Equation 11 is a calibration parameter for transverse bedslope effect and according to Baar et al. (2018),  $r$  ranges between 0.2 and 1.5 depending on sediment mobility and bedform characteristics. To keep the computation in the model as simple as possible and focus the study on investigating how tides affect the morphodynamics of bifurcation, a constant  $\alpha$  and  $r$  are applied (3 and 0.5) as also applied by Bolla Pittaluga, Coco, et al. (2015) and Iwantoro et al. (2021) in their 1D model. Meanwhile,  $h_{inp}$  is the depth of the source channel at the junction and  $h_{123}$  is the weighed average depth of the connected channels at the junction, expressed by

$$h_{123} = \frac{W_{inp} h_{inp} + W_{out1} h_{out1} + W_{out2} h_{out2}}{W_{inp} + W_{out1} + W_{out2}} \quad (14)$$

**Table 1**  
*Boundary Conditions, Model Settings and Some Dimensional Parameters for Two Continuous Simulations*

| $U_2/U_0$      | Initial depth (m) | Discharge ( $\text{m}^3\text{s}^{-1}$ ) | $w_1$ at bifurcation (m) | Tidal amplitude (m) | $L_w$ (km) | $L_c$ (km) | D50 (mm) | Morfac    | Tide-averaged froude nr. | Tide-averaged rouse nr. |
|----------------|-------------------|---|--------------------------|---------------------|------------|------------|----------|-----------|--------------------------|-------------------------|
| 0 (river-only) | 10                | 2,598–12,471                            | 250–1,200                | 0                   | Inf.       | 0          | 0.07–0.4 | 800       | 0.105                    | 0.48–12.63              |
| 0.4            | 10                | 292.65–1,877.85                         | 100–1,000                | 1                   | 15         | 10         | 0.07–0.5 | 800–2,000 | 0.096                    | 0.48–15.61              |
| 1.7            | 10                | 125.21–1,252.11                         | 100–1,000                | 1.5                 | 15         | 20         | 0.07–0.4 | 10–2,000  | 0.052                    | 0.48–12.63              |
| 3              | 10                | 32.3–165.03                             | 97–500                   | 1.5                 | 15         | 40         | 0.07–0.4 | 50–2,000  | 0.042                    | 0.48–12.63              |
| 5              | 6                 | 30.80–151.82                            | 94–500                   | 1.35                | 15         | 40         | 0.06–0.2 | 15–1,000  | 0.020                    | 0.36–5.17               |
| 9              | 4.5               | 27.87–132.91                            | 130–620                  | 1.5                 | 15         | 40         | 0.06–0.2 | 30–800    | 0.012                    | 0.36–5.17               |

*Note.* For each  $U_2/U_0$ , the equilibrium bed level was first calculated for a range of widths and grain sizes. Subsequently, this equilibrium was perturbed and the simulation was continued until it reached the new equilibrium.

where  $w_{\text{inp}}$  is the width of the source channel at the junction while  $w_{\text{out1}}$  and  $w_{\text{out2}}$  are the widths of the sink channels. In Equation 11,  $\vartheta'_{\text{inp}}$  is the grain-related Shields stress in the input channel at the junction and was calculated by

$$\vartheta' = \mu \vartheta \quad (15)$$

where  $\mu$  is an efficiency factor (van Rijn, 2007) and is calculated as  $\mu = (C/C')^2$ , in which  $C'$  is the grain related Chézy coefficient,

$$C' = 18 \log_{10}(12h/2.5D_{50}) \quad (16)$$

with  $D_{50}$  the median grain size of sediment (van Rijn, 1984a). Furthermore,  $\vartheta$  is total Shields stress,

$$\vartheta = \frac{(Q/A)^2}{\left(\frac{\rho_s}{\rho_w} - 1\right) C^2 D_{50}} \quad (17)$$

in which  $\rho_s$  and  $\rho_w$  are the density of sediment and water, respectively.  $\partial\eta/\partial y$  in Equation 11 is the transverse bed slope at the bifurcation calculated between the channel centers as:

$$\frac{\partial\eta}{\partial y} = \frac{\eta_{\text{out2}} - \eta_{\text{out1}}}{0.5w_{\text{inp}}} \quad (18)$$

Finally, the morphological change is computed using the sediment continuity equation and assumes a dynamic riverbed while the riverbanks are fixed:

$$w(1-p)\frac{\partial\eta}{\partial t} + \frac{\partial Q_s}{\partial x} = 0 \quad (19)$$

Here,  $p$  is the sediment porosity, which has a value of 0.35. The numerical scheme to solve Equation 19 was described in Iwantoro et al. (2021).

## 2.2. Model Set-Up

The schematized junction consists of an upstream channel of 80 km length and two downstream channels of 20 km length, discretized with spatial and time steps of 250 m and 5 min, respectively. The river discharge was imposed at upstream boundary applying a defined slope to calculate Equation 4 that was constant for all simulations in this study ( $3 \times 10^{-5}$ ) while a semi-diurnal tidal component with  $T_k$  of 12 hr was imposed at downstream boundaries. The location of these boundaries can be seen in Figure 1.

To investigate the stability of bifurcations as a function of tidal influence, we defined sets of simulations in which prescribed tidal amplitude and channel width profile were changed (Table 1). The tidal influence is indicated by the ratio of tidal flow amplitude ( $U_2$ ) over tide-averaged flow ( $U_0$ ) in the upstream channel at the bifurcation in

**Table 2**

Channel Geometry, Boundary Conditions and Morfac for Test Simulations to Study the Sensitivity of Equilibrium Bed to  $L_w$ ,  $L_c$ , River Discharge and  $D_{50}$

| Test case               | $L_w$ (km) | $L_c$ (km) | $D_{50}$ (mm) | Tidal amplitude (m) | Discharge ( $\text{m}^3\text{s}^{-1}$ ) | Initial depth (m) | $w_1$ at bifurcation (m) | Morfac | $U_2/U_0$ at equilibrium |
|-------------------------|------------|------------|---------------|---------------------|---|-------------------|--------------------------|--------|--------------------------|
| Sensitivity of $L_w$    | 15-Inf     | 20         | 0.25          | 1.5                 | 1,252–10,392.3                          | 10                | 1,000                    | 400    | 0–4                      |
| Sensitivity of $L_c$    | 15         | 20–40      | 0.25          |                     | 1,252–710.2                             |                   |                          | 220    | 0–3                      |
| Sensitivity of Q        | 15         | 20         | 0.25          |                     | 214.4–710.2                             | 4.5–10            |                          | 30–400 | 0–9                      |
| Sensitivity of $D_{50}$ | 15         | 20         | 0.1–0.4       |                     | 1,252                                   | 10                |                          | 200    | 0–1.7                    |

morphodynamic equilibrium (symmetric condition, not yet perturbed). Note that tidally averaged flow is caused by river discharge and by Stokes return flow and is nonzero for zero river discharge. We simulated conditions from  $U_2/U_0 = 0$  (river-only/no tide) to  $U_2/U_0 = 9$ . We prescribed the following width profile. The downstream channels are convergent over their entire length, which can be characterized by the e-folding length scale for width ( $L_w$ ). These converging channels are very typical for tidal systems (e.g., Davies & Woodroffe, 2010; Fagherazzi & Furbish, 2001; Langbein, 1963; Lanzoni & Seminara, 1998). The upstream channel is convergent until  $x = -L_c$ , after which the channel is straight until the upstream boundary:

$$w_{\text{upstream}} = \begin{cases} w_{1,0}e^{x/L_w}, & \text{for } -L_c < x \leq 0 \\ w_{1,0}e^{-L_c/L_w}, & \text{for } x \leq -L_c \end{cases} \quad (20)$$

$$w_{\text{downstream}} = w_{2,0}e^{x/L_w} = w_{3,0}e^{x/L_w}$$

Here,  $w_{1,0}$  is width of upstream channel at the junction, and  $w_{2,0}$  and  $w_{3,0}$  are the widths of both downstream channels at the junction, which in this study were defined as  $w_{2,0} = w_{3,0} = 0.5 w_{1,0}$ . Since  $w_{1,0}$  is self-defined, by changing  $L_c$  and  $L_w$ ,  $w_{1,ub}$  also changes. This affects the prescribed discharge according to Equation 4 and also the tidally averaged flow velocity at the bifurcation ( $U_0$ ). Furthermore,  $L_c$  and  $L_w$  affect the propagation of tides in the system. Similarly, river discharge (see Equation 4) and tidal propagation are also affected by the prescribed upstream water depth. As a result, beside defining a different tidal amplitude at seaward boundaries, we varied the tidal influence in the system by having different  $L_c$ ,  $L_w$  and initial depth.

For the design of channel shape, the effect of  $L_w$ ,  $L_c$ , river discharge and grain sizes on the equilibrium bed profile was studied. The settings for these simulations are shown in Table 2. These runs were also used to estimate conditions for which  $U_2/U_0$  at the bifurcations obtains a certain desired value. After this, two continuous simulations were conducted in which we aimed to simulate, for a certain value of  $U_2/U_0$ , the sensitivity of the results to width-to-depth ratio and Shields stress.

First, unperturbed simulations were conducted. We simulated the morphological evolution of a symmetric bifurcation until equilibrium (morphology is constant in time). This was followed by a set of simulations in which a perturbation was imposed on the symmetric equilibrium morphology. One downstream channel was deepened and the other one was made shallower by 1 cm and the perturbed system was simulated until a new equilibrium was achieved. We analyzed the depth asymmetry between both channels as a function of time, computed as

$$\Psi_h = \frac{\overline{h_3} - \overline{h_2}}{\overline{h_3} + \overline{h_2}} \quad (21)$$

where  $\overline{h_3}$  and  $\overline{h_2}$  are water depth averaged over the tidal cycle and over the entire branch length. A stable symmetric bifurcation is stable when the initially prescribed asymmetry decays, resulting in  $\Psi_h = 0$  in final equilibrium, while the symmetric bifurcation is unstable when the asymmetry grows, resulting in a non-zero  $\Psi_h$  (asymmetric bifurcation).

The sensitivity of the results to the width-to-depth ratio ( $w/h$ ) was studied by varying the width of the upstream channel at the bifurcation ( $w_{1,0}$ ), while the sensitivity to the grain related Shields stress was studied by varying the sediment grain size between 0.06 and 0.5 mm. This range of bed sediment size is within the range of observed



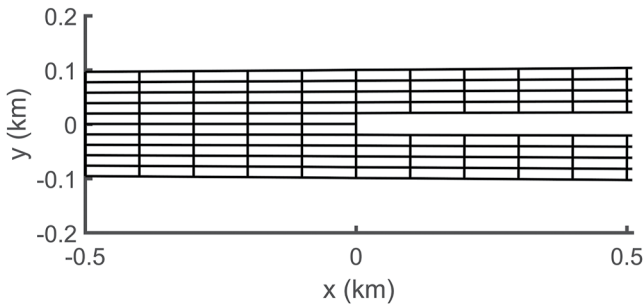


**Figure 3.** Close up of the numerical grid near the bifurcation for Delft3D model setup.

values in tide-influenced deltas and estuaries according to observations of several tidal systems (e.g., Buschman et al., 2013; Hoitink et al., 2017; Hu et al., 2009; Sassi et al., 2013; Stephens et al., 2017).

Other model parameters were the morphological acceleration factor and the Chézy bed roughness coefficient. Since morphological development is a long-term process that requires up to thousands of years until the bed level achieves a morphological equilibrium, we applied a parameter morphological acceleration factor (Morfac) to accelerate the morphological development (Lesser et al., 2004). The Morfac value applied depended on the model settings as shown in Tables 1 and 2. Regarding the bed roughness, a dimensionless Chézy coefficient was applied with the value of 20 ( $60 \text{ m}^{0.5} \text{ s}$  in dimensional form) as typically applied in tidal systems (Guo et al., 2015; Iwamoto et al., 2020; Xu et al., 2017). The channel configuration, boundary conditions and model settings for each simulation are shown in Table 1.

### 2.3. Validation of 1D Approach by Comparison With 2D Model

The 1D model results for hydrodynamics and morphodynamics were compared with a well-established 2D numerical model (Delft3D model). This was done to check whether the 1D model is able to simulate the morphological evolution for cases that flows reverse during a tidal cycle. We therefore compared the 1D model results to a case similar as described in Iwamoto et al. (2020). The numerical approach of the Delft3D model can be found in Lesser et al. (2004). The grid schematization to build a bifurcation followed the method of Kleinhans et al. (2008), in which the upstream channel was split by removing one node, or two grid cells, in the middle of the domain, as illustrated in Figure 3 (see also Iwamoto et al. (2020) for details). For the comparison, we applied settings and forcings from the simulation with  $U_2/U_0 = 3$ , as shown in Table 1 applying a w/h of 50 and  $D_{50}$  of 0.07 mm. This was a case for which the symmetric bifurcation is unstable and in final equilibrium the bed levels of the two downstream channels are asymmetric.

Regarding the hydrodynamics, the tide-averaged, semi-diurnal amplitude and its overtides (quarter- and sixth-diurnal amplitude) of water levels and flow velocities were compared for the symmetric case. No morphological update was included for the hydrodynamics comparison to prevent possible differences caused by different morphological evolution. The 1D results were compared with width-averaged values of the 2D model. The 1D model and 2D model show a fairly high correlation with  $r^2$  values above 0.97 for all tidal constituents, both for along-channel water levels and flow velocities.

Regarding the morphodynamical evolution, the symmetric case without bed perturbation shows a very similar bed level profile in both models, in which a downstream shallowing pattern occurs from the point where the channel starts to widen (Figure 4a). The 1D model has a bit deeper lying bed than the 2D model, but the difference is less than 1 m. The jump in bed level between upstream channel and downstream channels in Delft3D is due to the removal of two grid cells in the middle of the upstream channel, which caused a sudden reduction of channel width, starting at the bifurcation. Therefore, the bed level of the downstream channel compensates this width reduction resulting in a deepening of both downstream channels. As this width reduction was also applied to this 1D model run it likewise shows a sudden deepening after the bifurcation. After the bed levels of the symmetric bifurcation were perturbed and the bed evolution was simulated till a new equilibrium was achieved (Figure 4b), both models show similar bed level patterns and bed level asymmetry, in which the shallow downstream channel deepens in seaward direction while the deep shallows, and the depth difference between both channels is smaller downstream. While the model bed levels in the 1D model and 2D model are not exactly the same, the differences are acceptable and are caused by the fact that 2D model allows for variations in flow velocities and depth over the channel width. Because of the nonlinear feedbacks between flow and bed level this results in different width-averaged bed levels in the 1D and Delft3D model. The two models show some differences in the time series of morphological evolution of the downstream channels near the bifurcation (Figure 4c). Where Delft3D results show a gradual change until the new equilibrium, the 1D model shows a faster morphological change after 400 years. However, both models show a similar equilibrium depth of around 2.6 m for the shallow channel and 5.8 m for the deep one. Based on the comparison of the 1D and Delft3D model we conclude that the 1D model is able to simulate the morphodynamics of tide-influence bifurcations and can be used for further study.

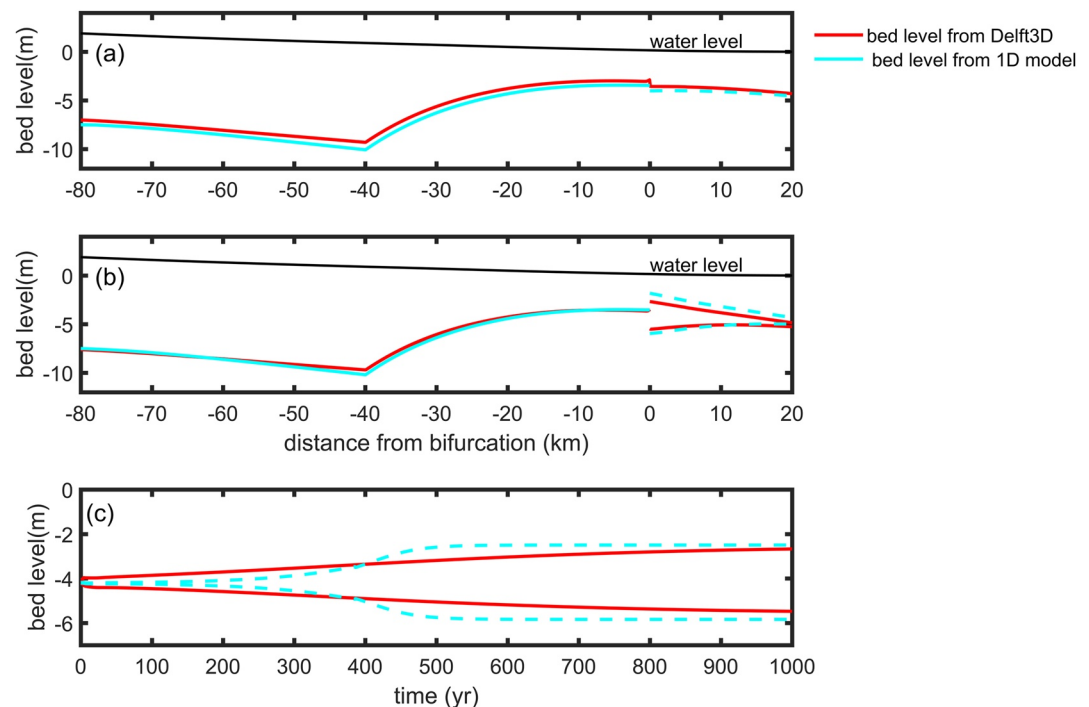


**Figure 4.** (a) Comparison of equilibrium morphology between the results of Delft3D (red line) and 1D model (cyan line) for symmetric bifurcation, Solid line is upstream channel and dashed lines represents morphology in downstream channels. Bifurcation is located at  $x = 0$ . (b) Same as (a), but now after a bed perturbation in downstream channels was applied. (c) Time series of the morphological development in the downstream channels at bifurcation after bed perturbation.

### 3. Results

#### 3.1. Effect of Channel Width Profile on Equilibrium Morphology of Symmetric Bifurcations

The sensitivity of the equilibrium channel depth profile to the channel width profiles was simulated for the symmetric conditions (unperturbed) for a system forced by both river flow and tides ( $S_2$  amplitude of 1.5 m). The e-folding length scale for channel width ( $L_w$ ) and the position where the upstream channel becomes straight ( $L_c$ ) strongly control the equilibrium morphology of the symmetric bifurcations (Figures 5a and 5b). Regarding the effect of  $L_w$  (Figure 5a), a straight channel ( $L_w = \text{inf}$ ) results in channel deepening in seaward direction, up to about 25 m at sea. This confirms results of Leuven et al. (2021), Ragno et al. (2020) and Bolla Pittaluga, Tambroni, et al. (2015), who also found that tides in straight channels cause deeper channels compared to river-dominated conditions. The strong tidal flow downstream and river discharge upstream results in an unrealistic deepening of the channels and larger tides result in a deeper equilibrium depth profile. When prescribing a converging channel width profile in the seaward portion of the system, the depth profile at equilibrium has a linear bed profile in the upstream part, until the point where the channel starts widening. The slope has a small dependence on the value of  $L_w$ . Seaward from the straight-converging transition point the channel starts shallowing. The converging channel width increases the tidal influence upstream while decreasing the river-induced flow velocities, and a smaller  $L_w$  (stronger convergence) results in a stronger tidal influence and a more pronounced shallowing of the channel at the seaward side, as is found in many estuaries. Furthermore, a larger  $L_c$ , results in the shallowing part of the system to shift more upstream (Figure 5b) while the depth at the mouth seems to be independent of  $L_c$ . The value of  $L_c$  mainly influences the river-induced flow velocities and thereby the relative strength of tidal currents compared to river flow. Thus, beside defining a smaller  $L_w$ , a stronger tidal influence can be achieved by defining a channel width profile with a larger  $L_c$ .

The equilibrium bed profile is also sensitive to the prescribed initial depth (Figure 5c) because its value influences the prescribed discharge upstream (Equation 4). Though the same tides were imposed for both simulations, the smallest discharge results in largest tidal influence ( $U_2/U_0 = 9$ , compared  $U_2/U_0 = 3$  for largest discharge) at the bifurcation and the bed profile is very different.

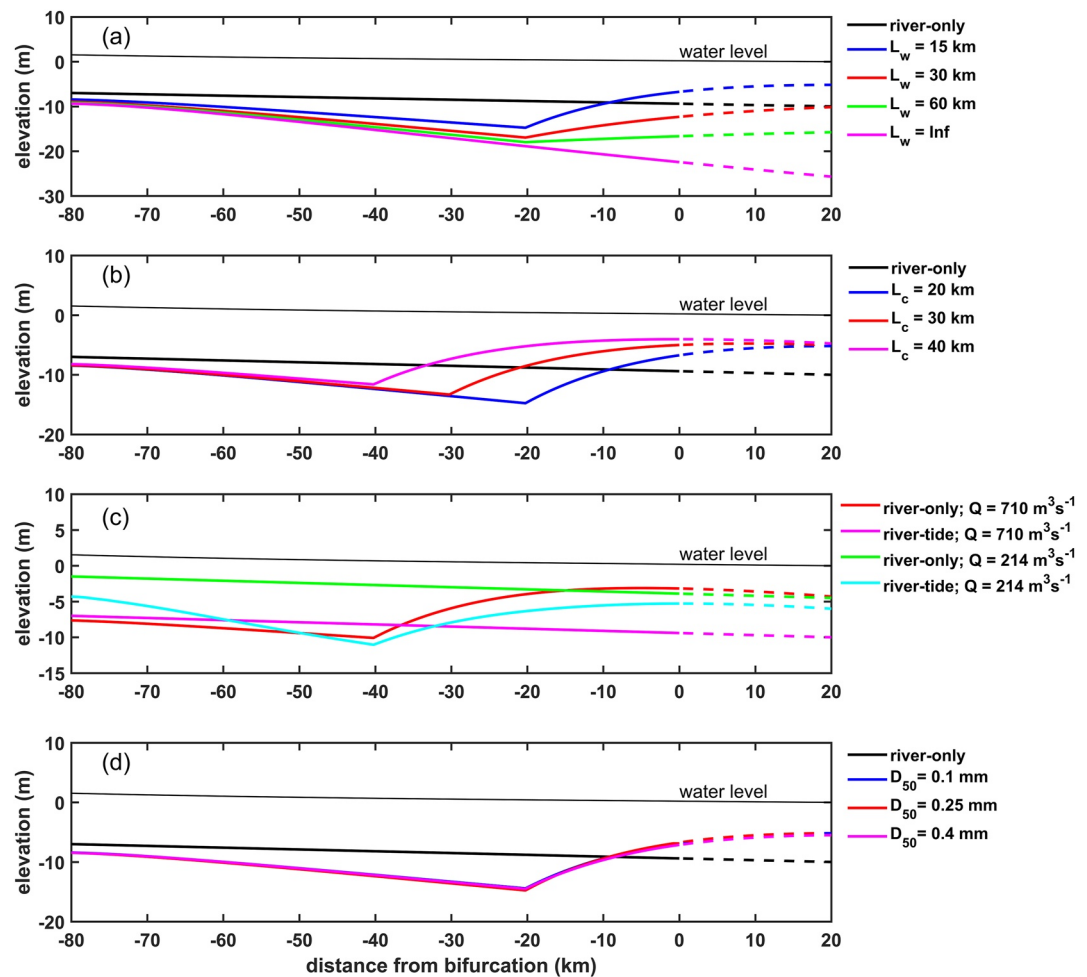


**Figure 5.** Equilibrium depth in all channels for the symmetric bifurcations for (a) different  $L_w$  with  $L_c = 20$  km; (b) different  $L_c$  with  $L_w = 15$  km and  $D_{50} = 0.25$  mm; (c) different discharge due to different initial depth; and (d) different values of  $D_{50}$  with  $L_w = 15$  km and  $L_c = 20$  km. All simulations applied  $S_2$  tidal amplitude of 1.5 m. The thick solid line indicates bed profile in the upstream channel while the dashed line is in downstream channels. The black (in (a), (b), and (d)); green; and magenta line (in (c)) are the equilibrium bed profile in river-only conditions (without tides and straight channel) and initial condition for simulations with tides.

In contrast to the channel width profile or upstream depth, the equilibrium bed profile is insensitive to the chosen grain size (Figure 5d). Thus, for the same tidal and river influence a change in grain sizes and therefore Shields stress will result in a similar equilibrium bed profile. Similarly, the equilibrium bed level of the symmetric bifurcations is also insensitive to the width at the bifurcation ( $w_{1,0}$ ) and therefore width-to-depth ratio. This is because we approximated the wetted perimeter to be equal to width of the channel, as described in Section 2. By doing this, the morphological equilibrium of a symmetric bifurcation with the same  $L_w$ ,  $L_c$  and initial depth but different channel width will be the same. The insensitivity of the equilibrium bed profiles to  $w_{1,0}$  and grain size allows for a systematic study of the stability properties of the symmetric bifurcations as a function of width-to-depth ratio and Shields stress, while the sensitivity of the results to tidal influence can be studied by changing the width profile or depth.

### 3.2. Stability and Asymmetry of Tide-Influenced Bifurcations

The stability of symmetric bifurcations is highly sensitive to the tidal influence in the system. Figure 6a shows the neutral stability curves, indicating the transition for which symmetric bifurcation are stable to depth perturbations (lower left-hand side of graph) and unstable (upper right-hand side). The neutral stability curves were obtained from the model for a range of tidal influences (indicated by  $U_2/U_0$ ) as a function of ebb-averaged width-to-depth

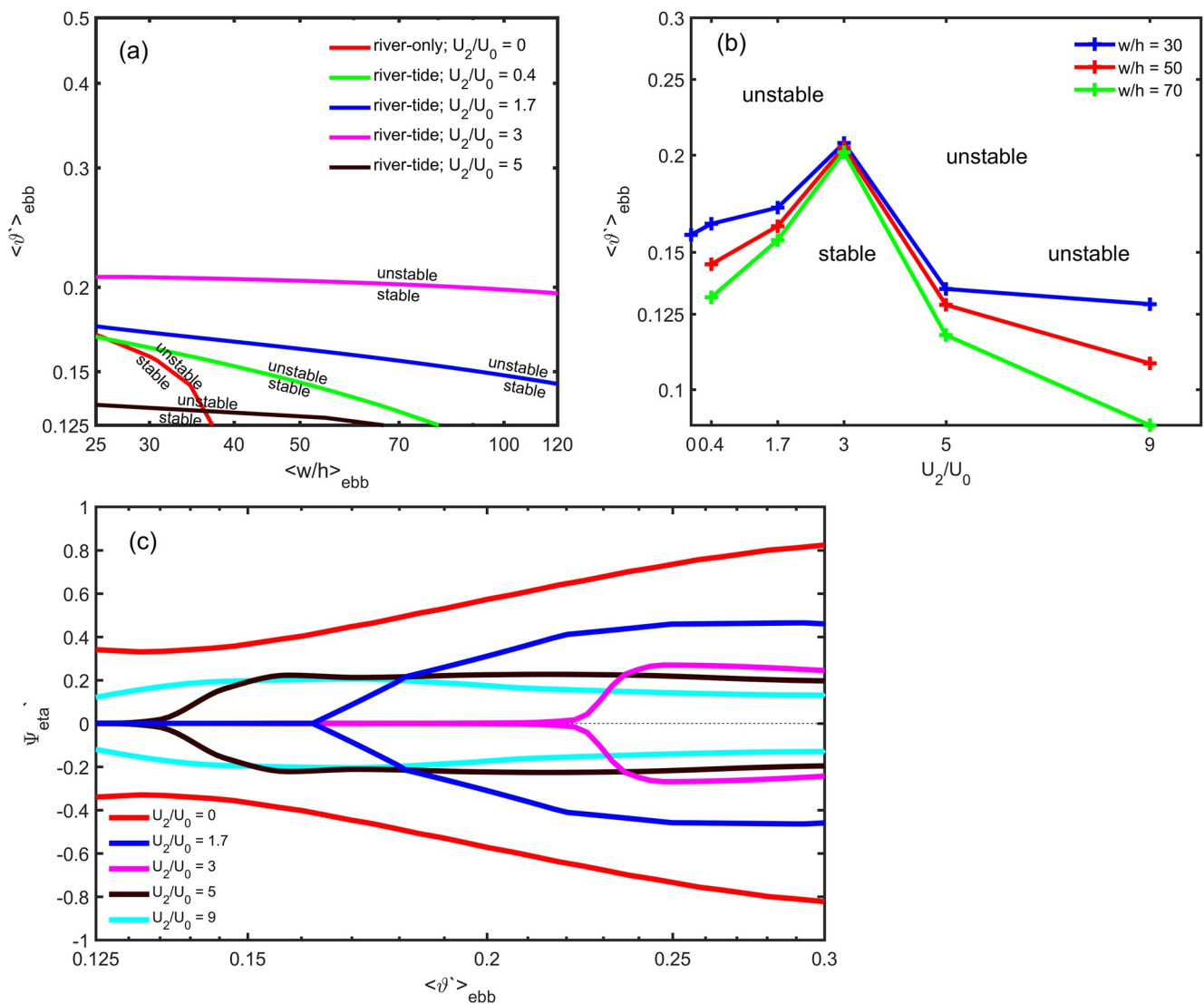


**Figure 6.** Neutral stability curves of symmetric bifurcations for a range of ebb-averaged grain-related Shields stress  $\langle \vartheta' \rangle_{ebb}$ : (a) as a function of ebb-averaged width-to-depth ratio ( $w/h$ ) for  $U_2/U_0$  of 0–5 and (b) as a function of  $U_2/U_0$ ; and (c) the bed level asymmetry between downstream channels in equilibrium for  $w/h$  of 50 and  $U_2/U_0$  of 0–9.

ratio  $w/h_{ebb}$  and the ebb-averaged grain-related Shields stress  $\vartheta'_{ebb}$  averaged over the ebb phase. Figure 6b shows the neutral stability curves for different ebb-averaged width-to-depth ratios as a function of tidal influence and the ebb-averaged grain-related Shields stress averaged over the ebb phase. The averaging over the ebb phase was considered to be more suitable than tide-averaging because of two reasons. First, ebb flow has the same flow direction as river flow and therefore the results from the set of simulations with  $U_2/U_0 < 1$  can be more easily compared to river-only bifurcations. Second, for the sets of simulations with low tidal influences (e.g.,  $U_2/U_0 = 1.7$ ), the Shields stress is nearly zero for several hours during rising tides. This is because the flood flow is counteracted by the river discharge. This would result in a small tide-averaged Shields stress, while it is clear that morphological change mainly takes place during ebb. Without the presence of tides ( $U_2/U_0 = 0$ ), symmetric bifurcations are stable in only a limited range of low Shields stress and small  $w/h$ . This is consistent with findings of Bolla Pitaluga et al. (2003), Redolfi et al. (2019) and Iwantoro et al. (2021). When forced by small tides, the range of conditions for stable symmetric bifurcations significantly expand to a much larger width-to-depth ratio value (Figure 6a). The larger  $U_2/U_0$  also results in a larger range of ebb-averaged Shields stress conditions with stable symmetric bifurcations, up till a maximum (Figure 6b). However, when the system becomes more tide dominated, indicated by the cases of  $U_2/U_0 = 5$  and 9, the opposite behavior occurs. The unstable conditions

expand to a much lower ebb-averaged values of Shields stress and  $w/h$ . As a result, only a limited stable regime exists, as shown for  $U_2/U_0 = 5$  in Figures 6a and 6b and for  $U_2/U_0 = 9$  in Figure 6b.

Besides having a strong influence on the range of conditions for which stable symmetric bifurcations occur, tides also reduce the final asymmetry for the unstable conditions. Figure 6c shows the asymmetry in equilibrium for a range of Shields stress conditions and tidal dominance, for  $w/h = 50$ . In the river-only case, asymmetric bifurcations occur for the entire range of Shields stress conditions, where the bed level asymmetry  $\Psi_h$  for higher Shields stress is close to 1, indicating a condition in which one of the two downstream channels will be abandoned. For the case of  $U_2/U_0 = 1.7$ , the asymmetry in unstable condition is about 50% smaller than for the river-only situation, and a range of conditions exist in which the bifurcation is stable to depth perturbations. For increasing tidal influence, the final asymmetry for the unstable symmetric conditions becomes increasingly smaller. Therefore, though the unstable symmetric bifurcations expand to a lower ebb-averaged Shields stress conditions for the most tide dominated conditions ( $U_2/U_0 = 5$  and 9), the final depth asymmetry shows a further reduction, with maximum values around 0.2. This results in bifurcations where both downstream channels continue to convey significant flow and sediment discharge.

### 3.3. Physical Mechanism Determining Stability of Bifurcations

We analyzed our simulations to study the intratidal dynamics that determine whether a symmetric bifurcation is stable or unstable. It turned out that during ebb the asymmetry of the bifurcation decays, while it grows during flood, as long as flow velocities during flood are above the threshold value. We analyzed the intratidal behavior of flow, sediment transport and morphological change for two cases that have similar hydrodynamics, but different sediment mobility due to different  $D_{50}$ . One case had a stable symmetric bifurcation, while the other was unstable to depth perturbation. For the unstable case the asymmetry decay during ebb could not compensate the asymmetry growth that occurred during flood, while for the stable case it did. Because the asymmetry index based on the most upstream nodes in the downstream channels ( $\Psi_{h,0}$ ) behaves similarly as the asymmetry index based on the spatial average of the bed level in each downstream channel ( $\Psi_h$ ), focusing on what happens near the bifurcation is sufficient.

Tides cause a time-varying sediment mobility (Figures 7a and 7b), width-to-depth ratio and  $\Psi_{h,0}$  (Figures 7c and 7d) when  $U_2/U_0 = 5$ . It can be seen that at flood the asymmetry grows. During ebb the asymmetry change is more variable in time, but it is mainly growing in the first part of the ebb (till 8h) and decreasing during the second part. The bed evolution in both channels ( $\partial Q_{s,0}/\partial x \approx -\partial \eta_{1,0}/\partial t$ ), shows that erosion and deposition (positive  $\partial Q_{s,0}/\partial x$  indicates erosion and negative  $\partial Q_{s,0}/\partial x$  indicates deposition) in both downstream channels occur simultaneously during a tidal cycle (Figure 7e and 7f), but at different rates, explaining the change in bed-level asymmetry.

#### 3.3.1. Asymmetry Growth During Flood

At early flood, deposition occurs in both downstream channels (Figures 7e and 7f). This is because during this phase, flood-directed flow velocities are larger seaward than they are landward resulting in a negative  $\partial Q_{s,0}/\partial x$ . The bed level asymmetry grows during this phase, because in the shallow channel deposition rate is faster than in the deep channel. Because in the deep channel the tides propagate faster than in the shallow channel, the tides tend to arrive earlier from the deeper channel. This causes spilling of water from the deep channel to the shallow channel (indicated by the interaction term of flow in Figure 8a), decreasing the spatial gradient in flow velocities (and thereby sediment transport) in the deep channel and increasing it in the shallow channel. This mechanism is illustrated in Figure 8a, where the interaction of flow between downstream channels induces a different spatial gradient of flow in both channels resulting in a development of bed level asymmetry. This asymmetry growth is more pronounced for the unstable symmetric case than for the stable case because the Shields stress is much larger for the unstable case, because of the smaller  $D_{50}$ . After the peak flood, the decreasing sediment mobility is followed by a decreasing deposition rate and in the late flood even erosion occurs, followed by a few hours without morphological change because Shields stress is too small to induce sediment transport. The same asymmetry change during flood is also found for  $U_2/U_0 = 3$ , (Figure A1 in the Appendix) but for  $U_2/U_0 = 1.7$  the flood flow is too weak to induce sediment transport (Figure A2 in the Appendix). We conclude that when flood flows are large enough to induce sediment transport, during the flood phase the bed level asymmetry grows.

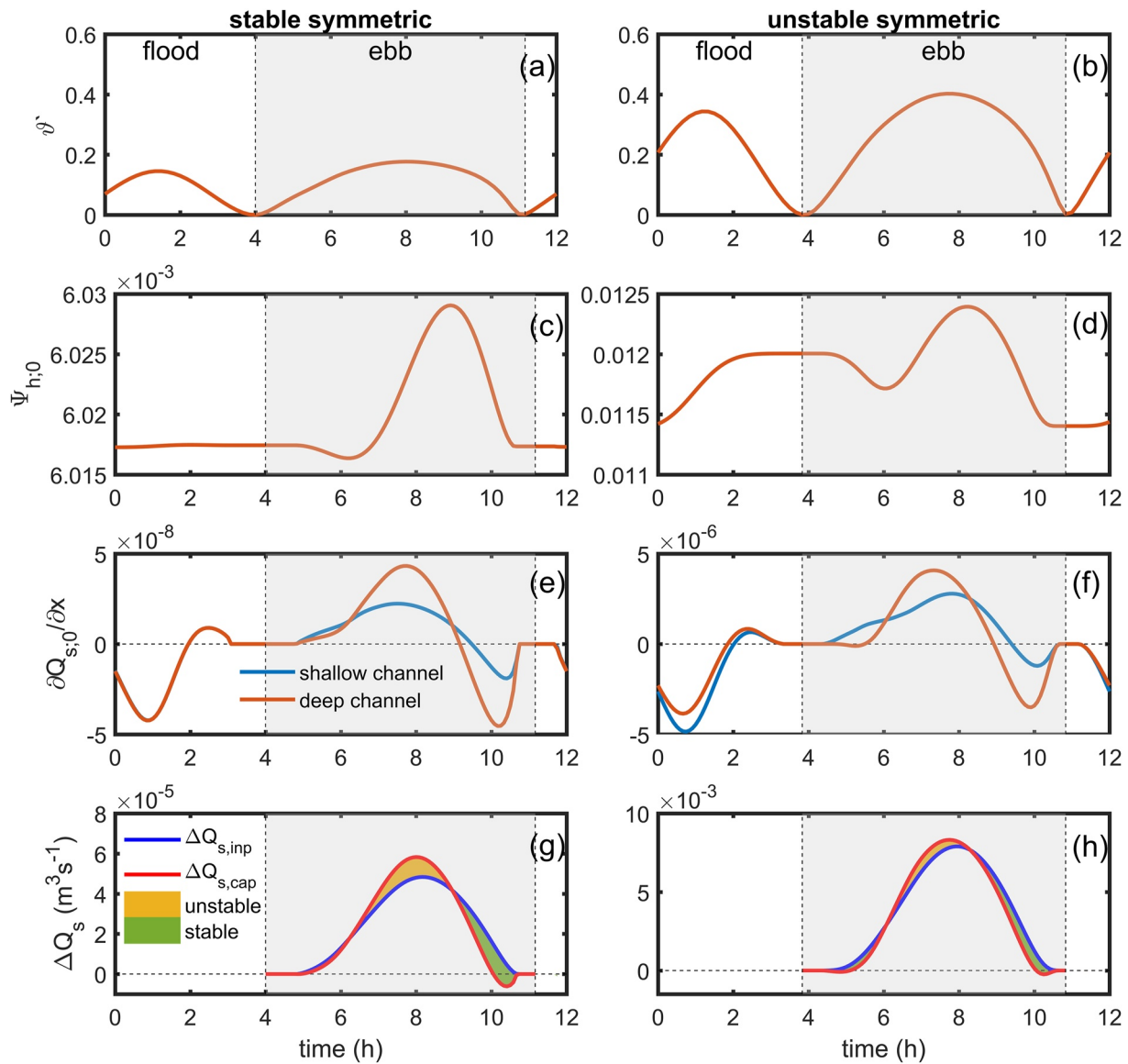


**Figure 7.** A fluctuation in a tidal cycle at the beginning of the simulation after the perturbation was imposed (the first 50 years) for: grain-related Shields stress ( $\theta'$ ) ((a) and (b)), bed level asymmetry at the most upstream grid in downstream channels ( $x = 0$ ) ((c) and (d)), sediment transport spatial gradient in downstream channels at  $x = 0$  ((e) and (f)), and sediment supply and capacity difference between downstream channels ((g) and (h)) for simulations with  $U_2/U_0 = 5$ ,  $\langle \theta' \rangle_{ebb} = 0.12$  (left panels),  $\langle \theta' \rangle_{ebb} = 0.26$  (right panels), and  $w/h = 50$ .

### 3.3.2. Asymmetry Change During ebb

During ebb, the morphodynamics in the downstream channels are determined by the sediment division at the bifurcation. At early ebb, both downstream channels have an increasing erosion rate. At these moment the ebb-directed flow velocities increase in seaward direction, explaining the erosive trend. This is followed by a decreasing erosion rate and even a phase with deposition, when ebb flow is declining (Figures 7e and 7f). However, the rate of bed level change in both downstream channels is different, which explains the change in bed level asymmetry in time. The temporal behavior of  $\Psi_{h,0}$  during ebb can be explained by the relation between the sediment transport capacity difference ( $\Delta Q_{s,cap}$ ) between both channels and sediment supply difference ( $\Delta Q_{s,inp}$ ) from upstream channel to both downstream channels (Figures 7g and 7h).  $Q_{s,cap}$  is the sediment transport capacity at the most upstream node in the downstream channels while  $Q_{s,inp}$  is the sediment supply from the upstream channel to each downstream channel that is computed by the nodal point relationship. When  $\Delta Q_{s,inp}$  is higher than  $\Delta Q_{s,cap}$  the bed level asymmetry between downstream channels decays, and otherwise it grows (Bolla Pittaluga,

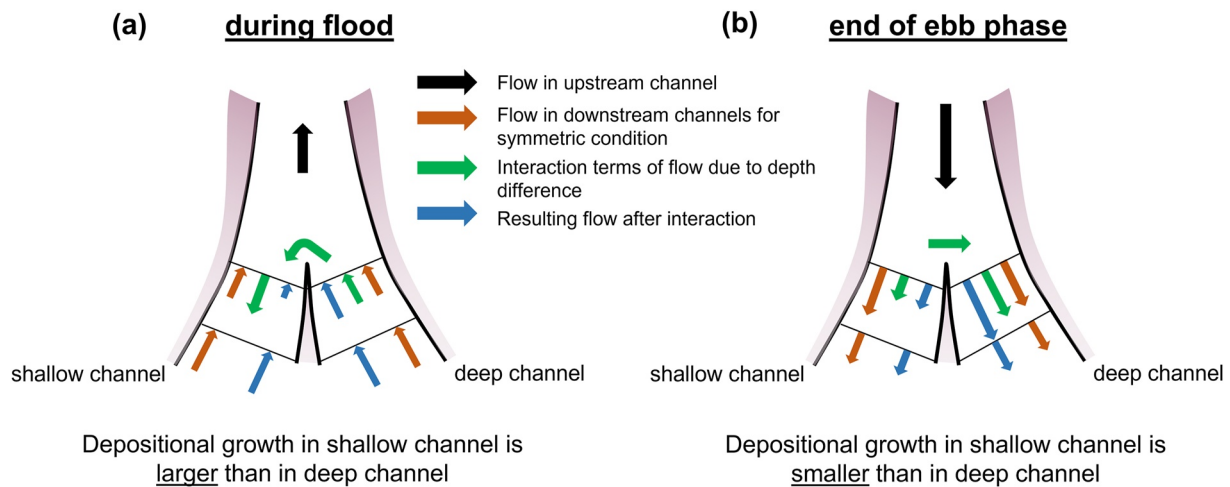


**Figure 8.** Mechanism of flow distribution at a bifurcation due to a depth difference between the downstream channels (defined perturbation) during (a) flood and (b) declining ebb flow, and its effect on the morphological development in the channels. Brown arrow indicates the symmetric flow condition when the bed level in the downstream channels is equal. After imposing bed level asymmetry between downstream channels, flow propagation from one downstream channel to the other (green arrow) occurs and results in a different spatial gradient of flow between downstream channels (blue arrow).

Coco, et al., 2015; Iwantoro et al., 2021). The differences between sediment supply and sediment transport capacity change in time during the ebb phase. At the beginning of ebb, when Shields stress is small,  $\Delta Q_{s, \text{inp}}$  compensates  $\Delta Q_{s, \text{cap}}$  and therefore reduces the asymmetry between downstream channels (Figures 7e and 7f). When the sediment mobility increases,  $\Delta Q_{s, \text{cap}}$  gradually exceeds  $\Delta Q_{s, \text{inp}}$ . The more rapid increase of  $\Delta Q_{s, \text{cap}}$  is due to the nonlinear dependence of sediment transport capacity on flow velocity. The flow velocity in deep channel is larger than in the shallow channel, for the same reason as why it is larger during flood. As a result, the erosion rate in deep channel is larger than in shallow channel and therefore the asymmetry between downstream channels increases. When ebb flow declines,  $\Delta Q_{s, \text{cap}}$  decreases more rapidly than  $\Delta Q_{s, \text{inp}}$  and at some point the asymmetry starts to decay. During this phase the flow velocity in the upstream channel is larger than in both downstream channels as the declining ebb flow is earlier downstream. Furthermore, there is this interaction flow from the shallow to the deep channel, which causes a relatively large supply of sediment to the deep channel (caused by the cross-channel flow component in the nodal point relation as indicated by the interaction term of flow in Figure 8b). This explains the relatively fast deposition occurring in the deep channel during this phase. The same asymmetry change during ebb is also found for the other tidal influence conditions as shown in Figure A1 for  $U_2/U_0 = 3$  and Figure A2 for  $U_2/U_0 = 1.7$  in the Appendix.

## 4. Discussion

### 4.1. Applicability of the 1D Model

In this study, a 1D morphodynamic model for bifurcations in river-dominated systems was extended to tide-influenced systems. Unlike earlier 1D models for tide-influenced systems (e.g., Jeuken & Wang, 2010; Zhang et al., 2014), the present 1D numerical model incorporates a nodal point relationship for sediment partitioning at bifurcation that considers transverse sediment transport when the sediment divides at the junction. Previous studies that used this approach were limited to river-dominated bifurcations (e.g., Bolla Pittaluga, Coco, et al., 2015; Iwantoro et al., 2021; Redolfi et al., 2019), or small tidal influence (Ragno et al., 2020) in which tides induce a changing flow magnitude but no change in direction ( $U_2/U_0 < 1$ ). In this study we developed the approach further to allow the nodal point relationship to be applied in tide-influenced systems in which the flow magnitude and direction can differ in each connected channels and change through time. As a result, this model can be applied for a wide range of tide-influenced conditions. We have shown that the outcome of the 1D model results in a similar morphological development as with a 2D model, but requires a much shorter simulation time at less computational cost. Therefore, this model is more suitable to investigate a long-term morphological development at the scale of tidal deltas. Furthermore, in this study we base our conclusions on 800 simulations, while the findings of Iwantoro et al. (2020) were based on 13 simulations. By having more simulations we investigated

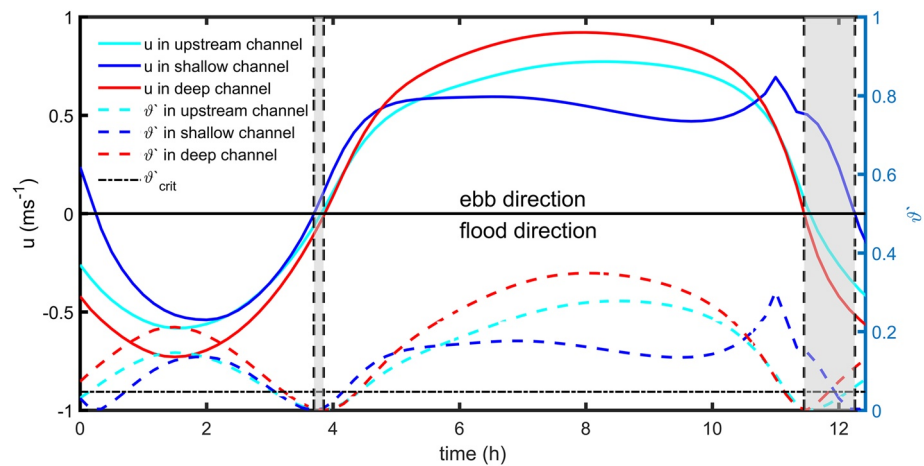


**Figure 9.** Intratidal behavior of flow ( $u$ ) and grain-related Shields stress ( $\theta'$ ) at the bifurcation in all channels for asymmetric equilibrium condition of 1D model and Delft3D comparison. The shaded area indicates the transition period between ebb and flood at which flow (a) merges from the downstream and upstream channel to the other downstream channel (indicated by negative (flood-direction)  $u$  in the deep downstream channel, and positive (ebb-direction)  $u$  in the upstream and the shallow downstream channel) and (b) divides from one downstream channel to the other two channels (indicated by positive  $u$  in the shallow downstream channel, and negative  $u$  in the upstream channel and the deep downstream channel). The dashed-dotted line indicates the critical Shields stress for sediment transport.

a wider range of sediment mobility, width-to-depth ratio and tidal influence than Iwamoto et al. (2020). As a result, in contrast to Iwamoto et al. (2020), this study found stable symmetric bifurcations with considerable tidal influence.

This study applied a new approach to compute sediment distribution at a bifurcation in unsteady flow conditions and can be applied in tide-influenced situations. It was assumed that the bed-slope driven sediment transport component can be scaled by the bed level differences between the different branches that connect at the junction and that it can immediately adapt when flow conditions change. However, in reality it may take time for this bedslope to develop, because it originates from a bar that develops at the junction (Redolfi et al., 2016; Salter et al., 2017). The comparison of the 1D model with the Delft3D simulations shows that this simplified approach works well, but further study is needed whether this is related to the fact that most of the time the flow was in a bifurcation condition in which water was flowing from the upstream channel to the two downstream ones as shown in Figure 9. The bifurcation condition at which the water flows from one of the downstream channel to the other two channels occurs when the depth between downstream channels is asymmetric and is limited to the transition between ebb and flood (shaded area in Figure 9). In this limited duration, the flow is small and therefore the sediment transport as well. When a situation occurs in which for a large portion of the tidal cycle water and sediment are flowing from one of the downstream channel to the other two channels also 3D flow effects can possibly be important, because the bifurcation angle is then very large. A vertical flow variation (3D effect) as presented, for instance, in Marra et al. (2014) and Lane et al. (1999) could become significant. However, in the 1D numerical model, this 3D effect is not taken into account (e.g., Bolla Pittaluga, Coco, et al., 2015; Kleinhans et al., 2012; Ragno et al., 2020). Field data is required for further study of the 3D effects in 1D models for tide-influenced bifurcations.

#### 4.2. Comparison With Previous Findings

The wider range of conditions for stable bifurcations for weak tidal influence systems as shown in this study were also found by Ragno et al. (2020). They proposed that the more stable symmetric condition occurs because fluctuation of tidal flow deepens the downstream channels and therefore reduces the imposed asymmetry between downstream channels. The deepening of the channels also causes the  $w/h$  ratio to become smaller, favoring stability. While we also found that channel deepening occurs during ebb flow, we found that the morphological asymmetry development in an ebb cycle is due to the changing dominance of sediment transport capacity and supply difference between the downstream channels. This study also confirms the finding by Iwamoto et al. (2020)



that the equilibrium asymmetry of bifurcations is lower for systems with more tidal influence. As a result, the unstable symmetric bifurcations would not lead to abandonment of one downstream channel as often found in river-dominated systems, but instead asymmetric bifurcations can exist in a wide range of conditions. This is consistent with observations in tide-influenced deltas, such as by Kästner and Hoitink (2019). It is interesting to note that predicted equilibrium asymmetry for  $U_2/U_0 > 5$  is in the order of 0.2 or even smaller. This implies that both channels will convey a considerable part of the tidal prism, river discharge and sediment transport, which has long-term ramifications for symmetry of delta progradation. In a purely fluvial situation with full channel avulsions, the delta only progrades around the mouth of active branches, but with tidal flows keeping both branches active, delta progradation would be more widespread and continuous.

The depth difference between downstream channels in the asymmetric bifurcations causes a partial tidal propagation from the deep channel to the shallow channel, as explained in the results section. This mechanism was also observed by Wagner and Mohrig (2019) in Wax Lake Delta where the tidal phase difference between downstream channels has caused a tidal propagation from one downstream channel to the other. Besides the phase difference they also observed a larger tidal flow amplitude in the channel that has the earlier tides as also shown in our model (Figure A3 in the Appendix). According to Iwantoro et al. (2020), the tidal propagation from one downstream channel to the other can lead to a development of subtidal trench at the bifurcation that connects the two downstream channels. This deepening at the bifurcation and tendency to keep both downstream channels open has also been observed in the Berau River Delta (Buschman et al., 2013).

While many tide-influenced channel networks exist without significant intertidal areas, many others do have extensive intertidal areas (Bain et al., 2019; Hiatt & Passalacqua, 2015). The presence of tidal flats could significantly change the asymmetry between flood and ebb flow. A larger tidal flat area in tidal systems generally leads to a more ebb-dominated condition (Pethick, 1980). This study has shown that flood flow increases the asymmetrical morphology between downstream channels. Defining tidal flats in the model may therefore reduce the influence of flood flow on the morphological development, which could lead to a broader range of conditions in which symmetric bifurcations are stable and a lower asymmetry between downstream channels for unstable symmetric conditions.

### 4.3. Future Directions

This study showed the effects of tides and proposed an explanation of the physical mechanisms that determine the morphological evolution of tide-influenced bifurcations, but future studies are still required to explain other important effects that could be important for the stability and asymmetry of tide influence bifurcations. We propose several promising research directions.

First, human interventions can significantly disturb the morphodynamics of tide-influenced bifurcations in deltas. Globally, deltas with their distributary channels have high ecological and economical values and are the center of populations (Ericson et al., 2006; Syvitski & Saito, 2007). Engineering works such as dredging-dumping activities for navigation, for example, in the ebb-flood channels of the Western Scheldt in the Netherlands (Jeuken & Wang, 2010) and the construction of short-cut channel between downstream branches of bifurcations could significantly influence the morphodynamics of these systems. Jeuken and Wang (2010) have, for example, shown that the equilibrium depth asymmetry between downstream channels can depend on the magnitude of the imposed initial perturbation. However, in their study the presence of transverse sediment transport at bifurcations that can compensate the asymmetry growth was not applied yet. This raises the questions whether transverse transport at a bifurcation can compensate the imposed asymmetry and whether there is a critical asymmetry threshold above which it cannot compensate the initial perturbation.

Second, sea level rise is important to the morphodynamics of bifurcations, especially in tide-influenced deltas. It changes tidal amplitude, tidal asymmetry and therefore the morphological response in the estuaries and deltas (Leuven et al., 2019; Prandle & Lane, 2015). Important questions are how and why sea level rise will affect the stability of bifurcations and their asymmetry. The deepening of the channel due to sea level rise increases the flood dominance (Wang et al., 2002) and different deposition rates in both downstream channels during flood, as shown in this study, may increase the asymmetry of the bifurcations. However, the morphological response during flood also depends on the relative importance of flood flow over ebb flow after sea level rises, so the effect is not clear yet.

Third, implementing movable channel banks in the model could further improve our knowledge about the morphodynamics in tide-influenced bifurcations. In tidal systems, tides induce morphological changes of the banks, resulting a converging channel width (as hypothesized in Savenije, 2015). This converging channel width provides feedback to the tidal propagation and affects the deformation of tides along the estuaries. In this study, the converging channel width was imposed. The effect of movable banks on tide-influenced bifurcations is unknown. However, effects of movable river banks in river dominated bifurcations were studied by Kleinhans et al. (2011) and Miori et al. (2006). They found that the unstable conditions for river bifurcations expand when the movable riverbanks are allowed in the model. This raises the question whether such an approach can be implemented in tide-influenced systems and whether this results in the same behavior as in river-dominated systems.

Fourth, in the model the transverse transport of suspended sediment at bifurcation is only driven by cross-channel flow, while in nature a diffusive transverse suspended load could also occur due to a transverse bed slope (Baar et al., 2018; Hepkema et al., 2019). This transverse suspended sediment transport could oppose the asymmetric morphological development between downstream channels during flood and ebb may lead to a wider range of conditions for where symmetric bifurcations are stable than presented in this paper. Besides, this mechanism may also result in a smaller bed level asymmetry for unstable symmetric bifurcation.

Lastly, many deltas in the world have complex channel networks formed by several junctions, such as in Mahakam Delta, Rhine-Meuse Delta and Mekong River Delta. Our model results suggest that tidal channel networks with two active channels are not ephemeral systems that develop slowly toward asymmetry and abandonment, but are in a stable condition. The more complex settings with more than two channels may lead to a significant asymmetric tidal propagation throughout the system. For instance, a length difference between downstream channels would impact the propagation of the tides and will result in differences in tidal flow velocities between channels. Furthermore, while we prescribed the same phase for the tides at the downstream boundaries, in reality both amplitude and phase can be different. We did not study these kind of externally forced asymmetries in this paper. Iwamoto et al. (2020) showed that increasing tidal influence will reduce the bed level asymmetry due to a length difference between downstream channels. They also found that a larger difference in tidal amplitude or phase prescribed at the two downstream channels results in a less asymmetric bifurcations. Simulating the hydrodynamics in the entire Mahakam Delta, Sassi et al. (2011) found that bifurcations closer to the sea have a higher tidal influence and have a less asymmetric tide-averaged discharge division between downstream channels. In contrast, using a series of simulations with a single, schematic bifurcation, Buschman et al. (2010) showed that tides increase this discharge asymmetry. This indirectly suggests that, beside affecting the flow distribution, the morphodynamics of bifurcations in a complex channel network may influence each other and induce an effect that cannot be captured by studying a single bifurcation. This leads to an open question whether the morphodynamics of an individual bifurcation in tide-influenced channel networks are influenced by the morphodynamical evolution of the other bifurcations.

## 5. Conclusions

Using a schematized bifurcation in a one-dimensional numerical model, this study showed the effects of tides on the stability and asymmetry of bifurcations in the range of river-to tide-dominated conditions and explained the mechanisms behind the effect of tides. We extend previous studies, which either focused on weak tides or were limited to few simulations, to tide-dominated conditions and explored a much larger parameter space. Compared with river-dominated systems, tides extend the conditions for which stable symmetric bifurcations can occur in mixed fluvial-tidal dominated systems, as long as the flood flow hardly drives morphological change. For these systems, the asymmetry change is determined by the ebb flows. For increasing tidal dominance, the smaller river discharge relative to the tidal discharge results in smaller peak ebb velocities and longer periods with low sediment mobility, and thereby cause symmetric systems to be stable. When tidal influence is increased above a certain optimum, the range of conditions for which symmetric bifurcations are stable becomes smaller again. We find that during flood the asymmetry grows. When the flood flow magnitude becomes comparable to the ebb flow magnitude, the asymmetry growth that occurs during flood cannot be compensated anymore during the ebb phase, and the bifurcation becomes unstable. However, although stronger tidal influence results in a more likely asymmetric development of the bifurcation, the final morphodynamical equilibrium becomes increasingly less asymmetric, confirming earlier findings. This keeps both downstream channels open and therefore prevents the tendency of abandonment of a downstream channel in tide-influenced bifurcations.

Appendix A

A1 Additional Figures: Mechanisms That Induce Morphological Development in Downstream Channel

Figure A1 and Figure A2 shows that the asymmetric development between downstream channels depends on the sediment transport fluctuation in the downstream channels for simulations with  $U_2/U_0 = 3$  and  $U_2/U_0 = 1.7$ , respectively. For the different tidal influence the most significant difference is during flood where the sediment mobility is larger for larger tidal influence (Figures A1a and A1b and Figures A2a and A2b). This also causes a larger asymmetric development during this phase (Figures A1c and A1d and Figures A2c and A2d) due to a larger morphological change (Figures A1e and A1f and Figures A2e and A2f). Meanwhile during ebb a similar asymmetry development occurs for different tidal influence that is mainly due to the relation between  $\Delta Q_{s,inp}$  than  $\Delta Q_{s,cap}$  (Figures A2g and A2h) where  $\Delta Q_{s,cap}$  is dominantly due to the asymmetry of tidal flow (Figure A3).

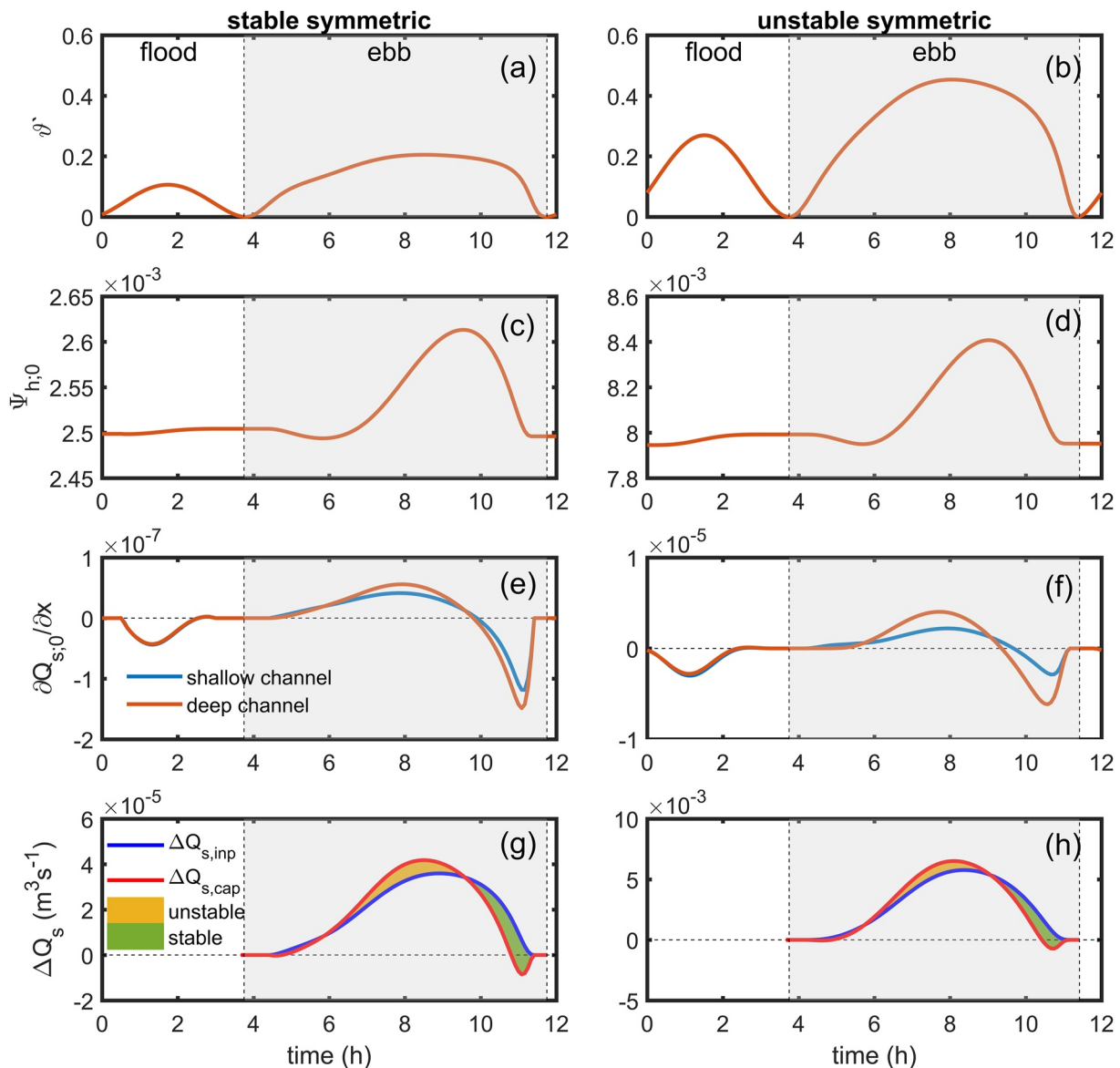


Figure A1. Same figure as Figure 7 for  $U_2/U_0 = 3$  at  $\langle \theta' \rangle_{ebb} = 0.15$  (right panels), and  $\langle \theta' \rangle_{ebb} = 0.25$  (left panels).

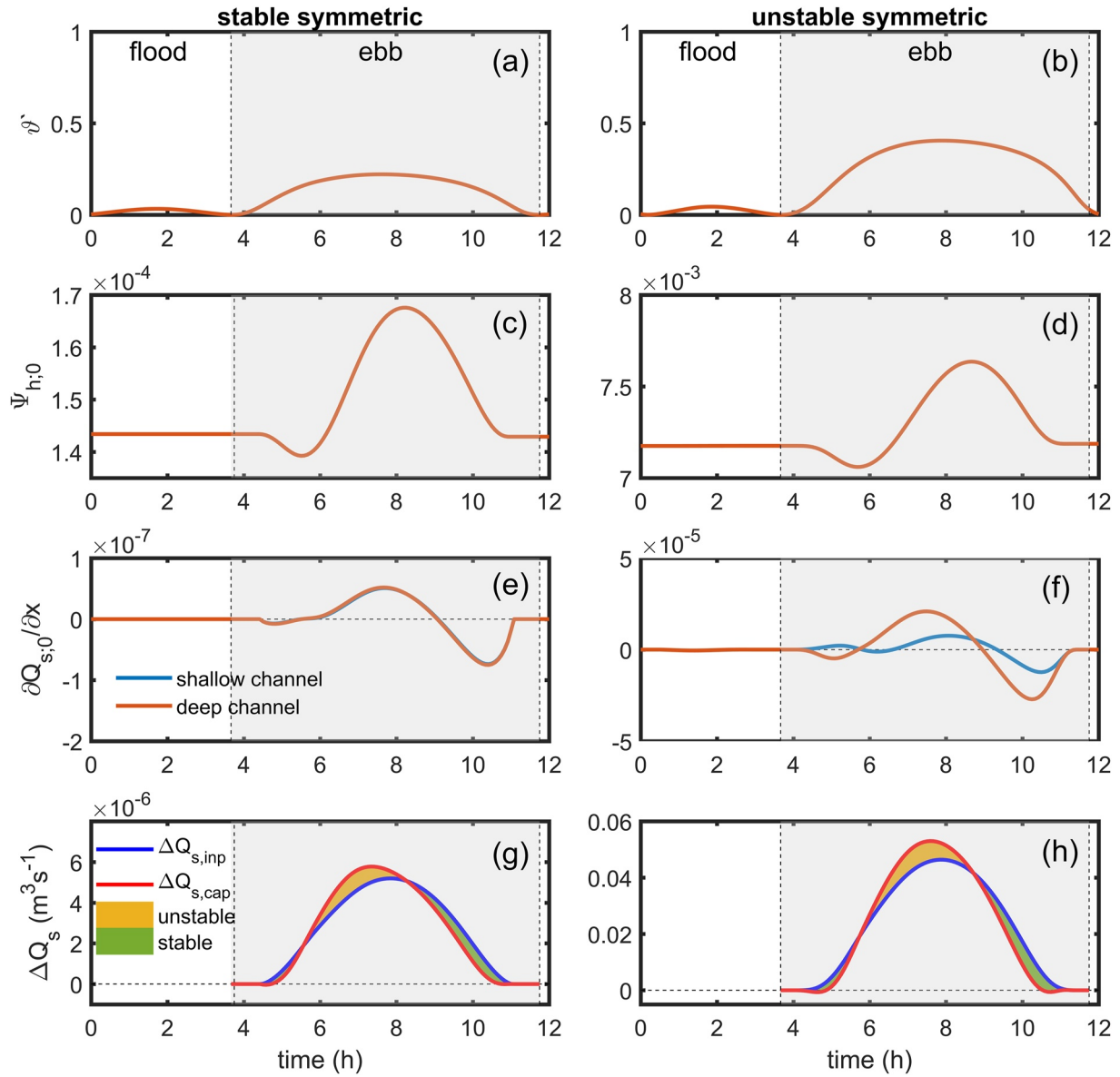
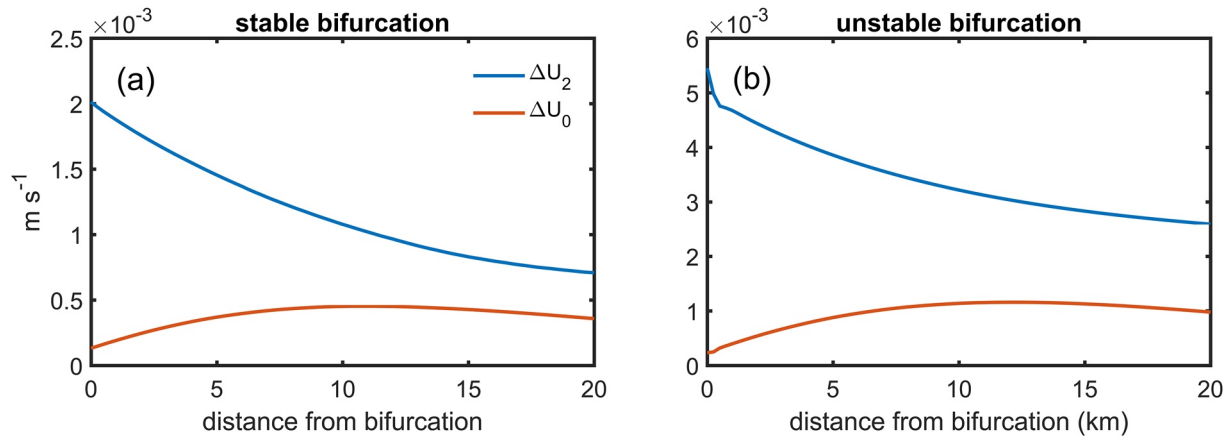


Figure A2. Same figure as Figure 7 for  $U_2/U_0 = 1.7$  at  $\langle \theta' \rangle_{ebb} = 0.15$  (right panels), and  $\langle \theta' \rangle_{ebb} = 0.45$  (left panels).



**Figure A3.** Tidal amplitude and tide-averaged flow velocity difference between deep and shallow downstream channel ( $\Delta U_2$  and  $\Delta U_0$ , respectively) along the channels for (a) stable and (b) unstable symmetric bifurcation at the beginning of simulation after perturbation was imposed (the first 50 years with  $U_2/U_0 = 5$ ,  $\langle \theta' \rangle_{ebb} = 0.12$  (left panels),  $\langle \theta' \rangle_{ebb} = 0.26$  (right panels), and  $w/h$  of 50).

### Notation

|                                 |  |
|---------------------------------|--|
| $\langle \theta' \rangle_{ebb}$ | ebb-averaged grain-related Shields stress at bifurcation in upstream channel |
| $\langle w/h \rangle_{ebb}$     | ebb-averaged width-to-depth ratio at bifurcation in upstream channel         |
| $A$                             | cross section area of the channel  |
| $a_k$                           | tidal amplitude  |
| $C$                             | total Chézy coefficient  |
| $C'$                            | grain-related Chézy coefficient  |
| $D_{50}$                        | median diameter of sediment  |
| $g$                             | gravitational acceleration   |
| $h$                             | water depth  |
| $L_c$                           | upstream distance from bifurcation where upstream channel width is funneling |
| $L_w$                           | e-folding length scale for width   |
| $P$                             | wetted perimeter of the channel cross section                                |
| $p$                             | sediment porosity  |
| $Q$                             | water discharge  |
| $Q_{bedl}$                      | bedload flux   |
| $Q_{bedl,y}$                    | transverse bedload flux at bifurcation                                       |
| $Q_s$                           | total sediment load  |
| $Q_{s,cap}$                     | sediment transport capacity  |
| $Q_{s,inp}$                     | sediment supply from upstream channel to downstream channels                 |
| $Q_{susp}$                      | suspended load flux  |
| $Q_{susp,y}$                    | transverse suspended load flux at bifurcation                                |
| $Q_y$                           | transverse water discharge   |
| $r$                             | empirical constant for transverse bed slope effect                           |
| $S$                             | channel slope  |
| $T_k$                           | tidal period   |
| $t$                             | time   |
| $U_0$                           | tide-averaged flow   |
| $U_{M2}$                        | tidal flow amplitude   |
| $w$                             | channel width  |
| $w_s$                           | sediment settling velocity   |
| $x$                             | spatial coordinate in streamwise direction                                   |
| $y$                             | spatial coordinate in transverse direction                                   |
| $z$                             | water level  |
| $\alpha$                        | dimensionless length of the region under bifurcation influence               |

|                            |   |
|----------------------------|---|
| $\Delta Q_{s, \text{cap}}$ | sediment transport capacity difference between downstream channels                    |
| $\Delta Q_{s, \text{inp}}$ | sediment supply difference between downstream channels                                |
| $\eta$                     | bed level   |
| $\theta$                   | total Shields stress  |
| $\theta'$                  | grain-related Shields stress  |
| $\mu$                      | efficiency factor for grain-related Shields stress                                    |
| $\xi$                      | Nikuradse roughness length related to the bedform                                     |
| $\rho_s$                   | sediment density  |
| $\rho_w$                   | water density   |
| $\varphi_k$                | tidal phase   |
| $\Psi_h$                   | asymmetry index of along channel- and tide-averaged depth between downstream channels |
| $\Psi_{h,0}$               | asymmetry index of tide-averaged depth between downstream channels at bifurcation     |
| $\omega_k$                 | tidal frequency   |

### Conflict of Interest

The authors declare no conflicts of interest relevant to this study.

### Data Availability Statement

The one-dimensional morphodynamic model code are available at [github.com/UtrechtRiversEstuaries/tidalnetwork\\_1D](https://github.com/UtrechtRiversEstuaries/tidalnetwork_1D). The model results to plot Figure 6 are available at repository via [figshare.com/s/597cd47d2c1d1ea77ce6](https://figshare.com/s/597cd47d2c1d1ea77ce6) with license: CC-BY 4.0.

### Acknowledgments

This research is funded by Indonesia Endowment Fund for Education (LPDP) grant to A.P. Iwantor (grant no.: 20161222029838).

### References

- Baar, A. W., de Smit, J., Uijtewaal, W. S. J., & Kleinhans, M. G. (2018). Sediment transport of fine sand to fine gravel on transverse bed slopes in rotating annular flume experiments. *Water Resources Research*, *54*(1), 19–45. <https://doi.org/10.1002/2017WR020604>
- Bain, R. L., Hale, R. P., & Goodbred, S. L. (2019). Flow reorganization in an anthropogenically modified tidal channel network: An example from the southwestern ganges-brahmaputra-meghna delta. *Journal of Geophysical Research: Earth Surface*, *124*(8), 2141–2159. <https://doi.org/10.1029/2018JF004996>
- Bertoldi, W., & Tubino, M. (2007). River bifurcations: Experimental observations on equilibrium configurations. *Water Resources Research*, *43*(10). <https://doi.org/10.1029/2007WR005907>
- Bertoldi, W., Zaroni, L., Miori, S., Repetto, R., & Tubino, M. (2009). Interaction between migrating bars and bifurcations in gravel bed rivers. *Water Resources Research*, *45*(6). <https://doi.org/10.1029/2008WR007086>
- Bolla Pittaluga, M., Coco, G., & Kleinhans, M. G. (2015). A unified framework for stability of channel bifurcations in gravel and sand fluvial systems. *Geophysical Research Letters*, *42*(18), 7521–7536. <https://doi.org/10.1002/2015GL065175>
- Bolla Pittaluga, M., Repetto, R., & Tubino, M. (2003). Channel bifurcation in braided rivers: Equilibrium configurations and stability. *Water Resources Research*, *39*(3), 1–13. <https://doi.org/10.1029/2003WR002754>
- Bolla Pittaluga, M., Tambroni, N., Canestrelli, A., Slingerland, R., Lanzoni, S., & Seminara, G. (2015). Where river and tide meet: The morphodynamic equilibrium of alluvial estuaries. *Journal of Geophysical Research: Earth Surface*, *120*(1), 75–94. <https://doi.org/10.1002/2014JF003233>
- Buschman, F. A., Hoitink, A. J. F., van der Vegt, M., & Hoekstra, P. (2010). Subtidal flow division at a shallow tidal junction. *Water Resources Research*, *46*(12), W12515. <https://doi.org/10.1029/2010WR009266>
- Buschman, F. A., van der Vegt, M., Hoitink, A. J. F., & Hoekstra, P. (2013). Water and suspended sediment division at a stratified tidal junction. *Journal of Geophysical Research: Oceans*, *118*(3), 1459–1472. <https://doi.org/10.1002/jgrc.20124>
- Chen, J. Y., Yun, C. X., & Xu, H. (1982). The model of development of the Changjiang estuary during the last 2000 years. *Proceedings of the Sixth Biennial International Estuarine Research Conference*, 655–666.
- Cunge, J. A., Holly, F. M., & Verwey, A. (1980). *Practical aspects of computational river hydraulics*. Pitman.
- Davies, G., & Woodroffe, C. D. (2010). Tidal Estuary width convergence: Theory and form in North Australian estuaries. *Earth Surface Processes and Landforms*. <https://doi.org/10.1002/esp.1864>
- Edmonds, D. A., & Slingerland, R. L. (2007). Mechanics of river mouth bar formation: Implications for the morphodynamics of delta distributary networks. *Journal of Geophysical Research*, *112*(F2), F02034. <https://doi.org/10.1029/2006JF000574>
- Edmonds, D. A., & Slingerland, R. L. (2008). Stability of delta distributary networks and their bifurcations. *Water Resources Research*, *44*(9). <https://doi.org/10.1029/2008WR006992>
- Ericson, J. P., Vörösmarty, C. J., Dingman, S. L., Ward, L. G., & Meybeck, M. (2006). Effective sea-level rise and deltas: Causes of change and human dimension implications. *Global and Planetary Change*, *50*(1–2), 63–82. <https://doi.org/10.1016/j.gloplacha.2005.07.004>
- Fagherazzi, S., & Furbish, D. J. (2001). On the shape and widening of salt marsh creeks. *Journal of Geophysical Research*, *106*(C1), 991–1003. <https://doi.org/10.1029/1999JC000115>
- Groen, P. (1967). On the residual transport of suspended matter by an alternating tidal current. *Netherlands Journal of Sea Research*, *3*(4), 564–574. [https://doi.org/10.1016/0077-7579\(67\)90004-X](https://doi.org/10.1016/0077-7579(67)90004-X)
- Guo, L., van der Wegen, M., Roelvink, D. J. A., Wang, Z. B., & He, Q. (2015). Long-term, process-based morphodynamic modeling of a fluvio-deltaic system, part I: The role of river discharge. *Continental Shelf Research*, *109*, 95–111. <https://doi.org/10.1016/j.csr.2015.09.002>

- Gurram, S. K., Karki, K. S., & Hager, W. H. (1997). Subcritical junction flow. *Journal of Hydraulic Engineering*, 123(5), 447–455. [https://doi.org/10.1061/\(asce\)0733-9429\(1997\)123:5\(447\)](https://doi.org/10.1061/(asce)0733-9429(1997)123:5(447))
- Hepkema, T. M., de Swart, H. E., & Schuttelaars, H. M. (2019). Sensitivity of tidal bar wavelength to channel width. *Journal of Geophysical Research: Earth Surface*, 124(10), 2417–2436. <https://doi.org/10.1029/2019JF005032>
- Hiatt, M., & Passalacqua, P. (2015). Hydrological connectivity in river deltas: The first-order importance of channel-island exchange. *Water Resources Research*, 51(4), 2264–2282. <https://doi.org/10.1002/2014WR016149>
- Hoitink, A. J. F., Wang, Z. B., Vermeulen, B., Huismans, Y., & Kästner, K. (2017). Tidal controls on river delta morphology. *Nature Geoscience*, 10(9), 637–645. <https://doi.org/10.1038/ngeo3000>
- Hu, K., Ding, P., Wang, Z., & Yang, S. (2009). A 2D/3D hydrodynamic and sediment transport model for the Yangtze Estuary, China. *Journal of Marine Systems*, 77(1–2), 114–136. <https://doi.org/10.1016/j.jmarsys.2008.11.014>
- Iwamoto, A. P., Van Der Vegt, M., & Kleinhans, M. G. (2020). Morphological evolution of bifurcations in tide-influenced deltas. *Earth Surface Dynamics*, 8(2), 413–429. <https://doi.org/10.5194/esurf-8-413-2020>
- Iwamoto, A. P., van der Vegt, M., & Kleinhans, M. G. (2021). Effects of sediment grain size and channel slope on the stability of river bifurcations. *Earth Surface Processes and Landforms*, 46(10), 2004–2018. <https://doi.org/10.1002/esp.5141>
- Jeuken, M. C. J. L., & Wang, Z. B. (2010). Impact of dredging and dumping on the stability of ebb-flood channel systems. *Coastal Engineering*, 57(6), 553–566. <https://doi.org/10.1016/j.coastaleng.2009.12.004>
- Kästner, K., & Hoitink, A. J. F. (2019). Flow and suspended sediment division at two highly asymmetric bifurcations in a river delta: Implications for channel stability. *Journal of Geophysical Research: Earth Surface*, 124(10), 2358–2380. <https://doi.org/10.1029/2018JF004994>
- Kleinhans, M. G., Cohen, K. M., Hoekstra, J., & Ijmker, J. M. (2011). Evolution of a bifurcation in a meandering river with adjustable channel widths, Rhine delta apex, The Netherlands. *Earth Surface Processes and Landforms*, 36(15), 2011–2027. <https://doi.org/10.1002/esp.2222>
- Kleinhans, M. G., de Haas, T., Lavooi, E., & Makaske, B. (2012). Evaluating competing hypotheses for the origin and dynamics of river anastomosis. *Earth Surface Processes and Landforms*, 37(12), 1337–1351. <https://doi.org/10.1002/esp.3282>
- Kleinhans, M. G., Jagers, H. R. A., Mosselman, E., & Sloff, C. J. (2008). Bifurcation dynamics and avulsion duration in meandering rivers by one-dimensional and three-dimensional models. *Water Resources Research*, 44(8), 1–31. <https://doi.org/10.1029/2007WR005912>
- Lane, S. N., Bradbrook, K. F., Richards, K. S., Biron, P. A., & Roy, A. G. (1999). The application of computational fluid dynamics to natural river channels: Three-dimensional versus two-dimensional approaches. *Geomorphology*, 29(1), 1–20. [https://doi.org/10.1016/S0169-555X\(99\)00003-3](https://doi.org/10.1016/S0169-555X(99)00003-3)
- Langbein, W. B. (1963). The hydraulic geometry of a shallow estuary. *International Association of Scientific Hydrology. Bulletin*, 8(3), 84–94. <https://doi.org/10.1080/0262666309493340>
- Lanzoni, S., & Seminara, G. (1998). On tide propagation in convergent estuaries. *Journal of Geophysical Research*, 103(C13), 30793–30812. <https://doi.org/10.1029/1998jc900015>
- Lentsch, N., Finotello, A., & Paola, C. (2018). Reduction of deltaic channel mobility by tidal action under rising relative sea level. *Geology*, 46(7), 599–602. <https://doi.org/10.1130/G45087.1>
- Lesser, G. R., Roelvink, J. a., van Kester, J. A. T. M., & Stelling, G. S. (2004). Development and validation of a three-dimensional morphological model. *Coastal Engineering*, 51(8–9), 883–915. <https://doi.org/10.1016/j.coastaleng.2004.07.014>
- Leuven, J. R. F. W., Pierik, H. J., van der Vegt, M., Bouma, T. J., & Kleinhans, M. G. (2019). Sea-level-rise-induced threats depend on the size of tide-influenced estuaries worldwide. *Nature Climate Change*, 9(12), 986–992. <https://doi.org/10.1038/s41558-019-0608-4>
- Leuven, J. R. F. W., van Keulen, D., Nienhuis, J. H., Canestrelli, A., & Hoitink, A. J. F. (2021). Large-scale scour in response to tidal dominance in estuaries. *Journal of Geophysical Research: Earth Surface*, 126(5). <https://doi.org/10.1029/2020JF006048>
- Marra, W. A., Parsons, D. R., Kleinhans, M. G., Keevil, G. M., & Thomas, R. E. (2014). Near-bed and surface flow division patterns in experimental river bifurcations. *Water Resources Research*, 50(2), 1506–1530. <https://doi.org/10.1002/2013WR014215>
- Miori, S., Repetto, R., & Tubino, M. (2006). A one-dimensional model of bifurcations in gravel bed channels with erodible banks. *Water Resources Research*, 42(11). <https://doi.org/10.1029/2006WR004863>
- Pethick, J. S. (1980). Velocity surges and asymmetry in tidal channels. *Estuarine and Coastal Marine Science*, 11(3), 331–345. [https://doi.org/10.1016/S0302-3524\(80\)80087-9](https://doi.org/10.1016/S0302-3524(80)80087-9)
- Postma, H. (1961). Transport and accumulation of suspended matter in the Dutch Wadden Sea. *Netherlands Journal of Sea Research*, 1(1–2), 148–190. [https://doi.org/10.1016/0077-7579\(61\)90004-7](https://doi.org/10.1016/0077-7579(61)90004-7)
- Prandle, D., & Lane, A. (2015). Sensitivity of estuaries to sea level rise: Vulnerability indices. *Estuarine, Coastal and Shelf Science*, 160, 60–68. <https://doi.org/10.1016/j.ecss.2015.04.001>
- Pritchard, D., & Hogg, A. J. (2003). Cross-shore sediment transport and the equilibrium morphology of mudflats under tidal currents. *Journal of Geophysical Research*, 108(C10), 3313. <https://doi.org/10.1029/2002jc001570>
- Ragno, N., Redolfi, M., & Tubino, M. (2021). Coupled morphodynamics of river bifurcations and confluences. *Water Resources Research*, 57(1). <https://doi.org/10.1029/2020WR028515>
- Ragno, N., Tambroni, N., & Bolla Pittaluga, M. (2020). Effect of small tidal fluctuations on the stability and equilibrium configurations of bifurcations. *Journal of Geophysical Research: Earth Surface*, 125(8). <https://doi.org/10.1029/2020JF005584>
- Redolfi, M., Zolezzi, G., & Tubino, M. (2016). Free instability of channel bifurcations and morphodynamic influence. *Journal of Fluid Mechanics*, 799, 476–504. <https://doi.org/10.1017/jfm.2016.389>
- Redolfi, M., Zolezzi, G., & Tubino, M. (2019). Free and forced morphodynamics of river bifurcations. *Earth Surface Processes and Landforms*, 44(4), 973–987. <https://doi.org/10.1002/esp.4561>
- Rossi, V. M., Kim, W., López, J. L., Edmonds, D., Geleynse, N., Olariu, C., et al. (2016). Impact of tidal currents on delta-channel deepening, stratigraphic architecture, and sediment bypass beyond the shoreline. *Geology*, 44(11), 927–930. <https://doi.org/10.1130/G38334.1>
- Salter, G., Paola, C., & Voller, V. R. (2017). Control of delta avulsion by downstream sediment sinks. *Journal of Geophysical Research: Earth Surface*, 123(1), 142–166. <https://doi.org/10.1002/2017JF004350>
- Salter, G., Voller, V. R., & Paola, C. (2020). *Chaos in a simple model of a delta network*. Proceedings of the National Academy of Sciences of the United States of America. <https://doi.org/10.1073/pnas.2010416117>
- Sassi, M. G., Hoitink, A. J. F., De Brye, B., Vermeulen, B., & Deleersnijder, E. (2011). Tidal impact on the division of river discharge over distributary channels in the Mahakam Delta. *Ocean Dynamics*, 61(12), 2211–2228. <https://doi.org/10.1007/s10236-011-0473-9>
- Sassi, M. G., Hoitink, A. J. F., Vermeulen, B., & Hidayat, H. (2013). Sediment discharge division at two tidally influenced river bifurcations. *Water Resources Research*, 49(4), 2119–2134. <https://doi.org/10.1002/wrcr.20216>
- Savenije, H. H. G. (2015). Prediction in ungauged estuaries: An integrated theory. *Water Resources Research*, 51(4), 2464–2476. <https://doi.org/10.1002/2015WR016936>

- Slingerland, R., & Smith, N. D. (1998). Necessary conditions for a meandering-river avulsion. *Geology*, 26(5), 435–438. [https://doi.org/10.1130/0091-7613\(1998\)026<0435:NCFAMR>2.3.CO;2](https://doi.org/10.1130/0091-7613(1998)026<0435:NCFAMR>2.3.CO;2)
- Stephens, J. D., Allison, M. A., DiLeonardo, D. R., Weathers, H. D., Ogston, A. S., McLachlan, R. L., et al. (2017). Sand dynamics in the Mekong River channel and export to the coastal ocean. *Continental Shelf Research*, 147, 38–50. <https://doi.org/10.1016/j.csr.2017.08.004>
- Syvitski, J. P. M., & Saito, Y. (2007). Morphodynamics of deltas under the influence of humans. *Global and Planetary Change*, 57(3–4), 261–282. <https://doi.org/10.1016/j.gloplacha.2006.12.001>
- van Rijn, L. C. (1984a). Sediment transport, part I: Bed load transport. *Journal of Hydraulic Engineering*, 110(10), 1431–1456. [https://doi.org/10.1061/\(ASCE\)0733-9429\(1984\)110:10\(1431\)](https://doi.org/10.1061/(ASCE)0733-9429(1984)110:10(1431))
- van Rijn, L. C. (1984b). Sediment transport, part II: Suspended load transport. *Journal of Hydraulic Engineering*, 110(11), 1613–1641. [https://doi.org/10.1061/\(ASCE\)0733-9429\(1984\)110:11\(1613\)](https://doi.org/10.1061/(ASCE)0733-9429(1984)110:11(1613))
- van Rijn, L. C. (2007). Unified view of sediment transport by currents and waves. II: Suspended transport. *Journal of Hydraulic Engineering*, 133(6), 668–689. [https://doi.org/10.1061/\(asce\)0733-9429\(2007\)133:6\(668\)](https://doi.org/10.1061/(asce)0733-9429(2007)133:6(668))
- van Straaten, L. M. J. U., & Kuenen, P. H. (1958). Tidal action as a cause of clay accumulation. *SEPM Journal of Sedimentary Research*, 28(4), 406–413. <https://doi.org/10.1306/74d70826-2b21-11d7-8648000102c1865d>
- Wagner, W., & Mohrig, D. (2019). Flow and sediment flux asymmetry in a branching channel delta. *Water Resources Research*, 55(11), 9563–9577. <https://doi.org/10.1029/2019WR026050>
- Wang, Z. B., De Vries, M., Fokkink, R. J., & Langerak, a. (1995). Stability of river bifurcations in 2D morphodynamic models. *Journal of Hydraulic Research*, 33(6), 739–750. <https://doi.org/10.1080/00221689509498549>
- Wang, Z. B., Jeuken, M. C. J. L., Gerritsen, H., De Vriend, H. J., & Kornman, B. A. (2002). Morphology and asymmetry of the vertical tide in the westerschelde estuary. *Continental Shelf Research*, 22(17), 2599–2609. [https://doi.org/10.1016/S0278-4343\(02\)00134-6](https://doi.org/10.1016/S0278-4343(02)00134-6)
- Xu, F., Coco, G., Zhou, Z., Tao, J., & Zhang, C. (2017). A numerical study of equilibrium states in tidal network morphodynamics. *Ocean Dynamics*, 67(12), 1593–1607. <https://doi.org/10.1007/s10236-017-1101-0>
- Zhang, W., Jia, Q., & Chen, X. (2014). Numerical simulation of flow and suspended sediment transport in the distributary channel networks. *Journal of Applied Mathematics*, 2014, 1–9. <https://doi.org/10.1155/2014/948731>